A 2+1 Dimensional Insoluble Surfactant Model for a Vertical Draining Free Film

By SHAILESH NAIRE[1]†, RICHARD J. BRAUN[1]‡ AND STEVEN A. SNOW[2]

[1]Department of Mathematical Sciences, University of Delaware, Newark, DE 19716, USA

[2]Interfacial Expertise Center, Dow Corning Corporation, Midland, MI 48686-0994, USA

(Received 9 May 2002)

A 2+1 dimensional mathematical model is constructed to study the evolution of a vertically-oriented thin, free liquid film draining under gravity when there is an insoluble surfactant, with finite surface viscosity, on its free surface. Lubrication theory for this free film results in four coupled nonlinear partial differential equations (PDEs) describing the free surface shape, the surface velocities and the surfactant transport, at leading order. Numerical experiments are performed to understand the stability of the system to perturbations across the film. In the limit of large surface viscosities, the evolution of the free surface is that of a rigid film. In addition, these large surface viscosities act as stabilizing factors due to their energy dissipating effect. An instability is seen for the mobile case; this is caused by a competition between gravity and the Marangoni effect. The behavior observed from this model qualitatively matches some structures observed in draining film experiments.

---

† Present address: Division of Theoretical Mechanics, University of Nottingham, UK

‡ Corresponding author, fax (302)831-4511; email: braun@math.udel.edu

1. Introduction

In this paper, we develop a mathematical model to simulate a vertically-aligned thin liquid film with an insoluble surfactant draining under gravity. Motivation for this study comes from a draining film experiment developed by Snow and co-workers (Snow & Stevens 1999; Snow, Nugent & Pernisz 1996*a*,*b*; Snow, Nugent, Pernisz, Naire & Braun 1996*c*; Snow, Pernisz & Stevens 1998) at Dow Corning. In this experiment, a rectangular frame is lifted to a fixed height above a cuvette of liquid. This allows for the suspension of a thin liquid film from the wire frame to the bath in the cuvette, and its subsequent drainage due to gravity back into the bath. The bath in the cuvette at the bottom models a Plateau border; the top of the film models the middle of a film in a foam. The experiment typically uses polyether/toluene blend that is 80 times more viscous than water and behaves as a Newtonian fluid; silicone surfactants are added and evaluated in the experiment. This model experiment has gravity driven drainage competing with various surface forces caused by film deformation and the presence of surfactant; thus, the necessary elements to model thin liquid film drainage in foams are present. The amount and type of surfactant affect the drainage rate and commercially successful surfactants have been used as benchmarks in the experiments. The experiments use interferometry to measure the rate of thinning of the film and can give detailed information about the shape of the surface of the film.

Figures 1(a–d) are a sequence of fringe patterns at time approximately equal to 1.5, 2.5, 3.5 and 4.5 minutes after film formation, respectively. These fringe patterns depict many of the physical features of polyurethane (PU) films. Flows can be observed in the film, concentrated at the bottom of the film and along the sides and top edges. The finger-like patterns at the bottom of the film proceed upward along the film. The structures along the edges of the film also move upward, except for those at the top edge

which proceed inwards from the sides of the film. These patterns are larger and slower moving compared to those found in aqueous films, e.g., Baets & Stein and plate II of Mysels, Shinoda & Frankel (1959). Some of the important conclusions that were arrived at from the experimental observations were that the temporal rate of change of fringe density and rate of movement of the finger-like patterns could be correlated to the film drainage rate. In some cases, the observation of rigid-surfaced films could be attributed to the large surface viscosity of the particular surfactant used (Snow *et al.* 1996*a*). The drainage rate of the film could be correlated to the surface viscosity. In cases of low surface viscosity, the extensive, relatively fast-moving and complex flow patterns on the surface of the flow were attributed to the Marangoni effect; surface flows stimulated by surface tension gradients. The chaotic appearance of the flows was attributed to the fact that two directionally opposite flow processes were present; the shear flow of the surface due to film drainage and the opposing Marangoni flow (Snow *et al.* 1998).

Mysels *et al.* were the first to investigate different types of thin film drainage in vertical aqueous soap films. They observed mobile films that showed edge turbulence and upward swirling flows and rigid films that showed little or no motion. They proposed that the turbulent motion and rapid drainage, which presumably play a major role in the thinning of mobile films, were the result of marginal regeneration. This refers to the flow in the Plateau border regions, where thin spots of film are generated and thicker spots disappear. This exchange of thinner for thicker film elements results in an effective drainage of the film. According to them, marginal regeneration is a consequence of variations in the thickness-averaged density of the film leading to a replacement of thicker film elements by thinner ones.

Hudales & Stein (1989, 1990), while experimentally testing the hydrodynamic theory for the above concept of marginal regeneration, measured profiles of the Plateau border at

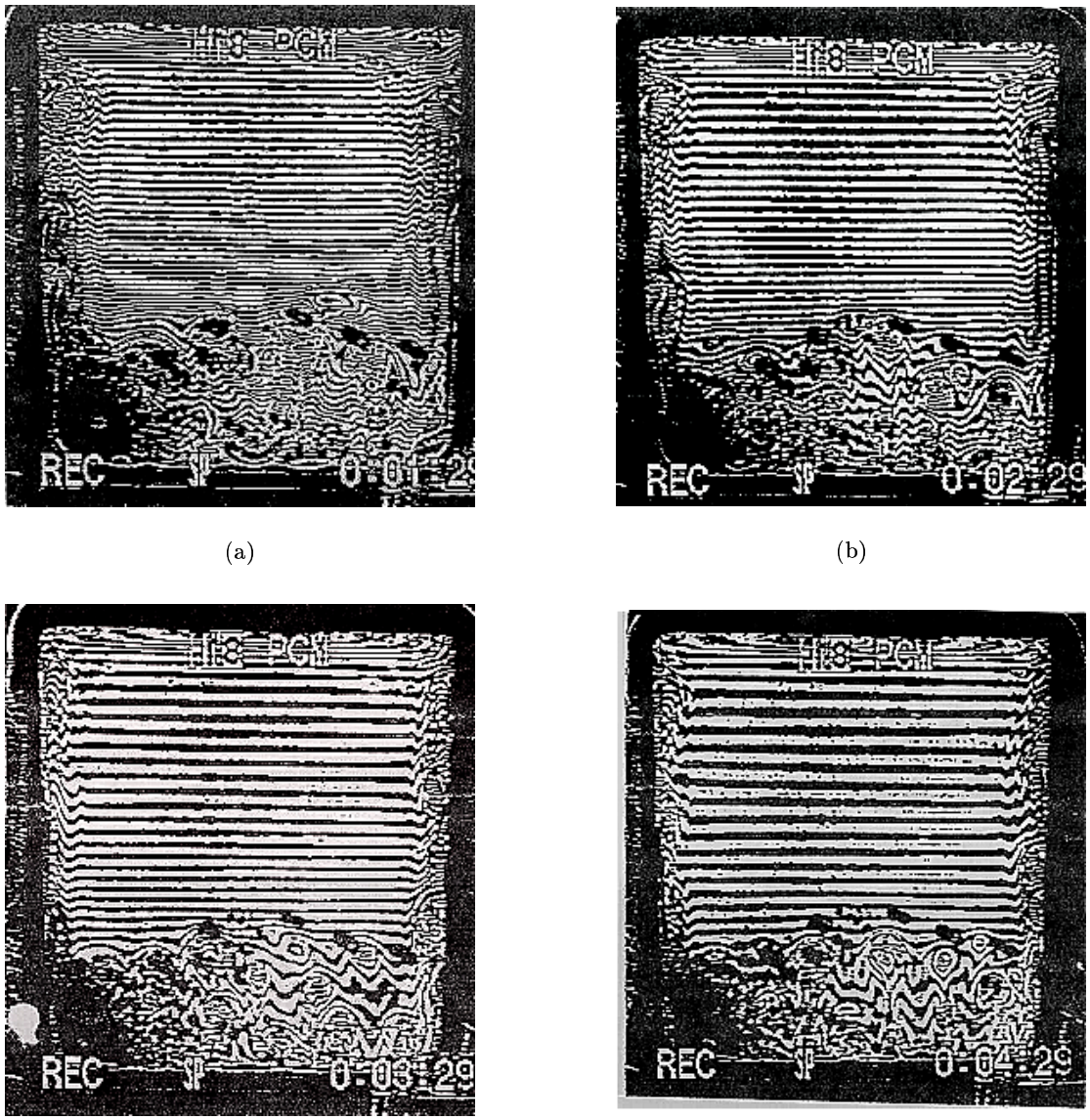

(a) (b)

(c) (d)

FIGURE 1. Sequence of fringe patterns at (a) $\bar{t} \approx 1.5$ minutes, (b) $\bar{t} \approx 2.5$ min., (c) $\bar{t} \approx 3.5$ min. and (d) $\bar{t} \approx 4.5$ min., where $\bar{t}$ is dimensional time. The topmost part of each fringe pattern is where the film is fixed to the wire frame; the bottom is where the film enters the bath; the fringe area is roughly 1cm×1cm. As $\bar{t}$ increases, fewer fringes are present which suggests film thinning due to drainage. Fringes in the middle region are roughly horizontal and uniformly spaced which suggests a two dimensional film shape and a roughly planar film surface in this region. Surface flows are seen near the bottom and along the sides. The finger-like patterns seen at the bottom and along the sides are much bigger and slower moving than that seen in aqueous soap film experiments by Mysels *et al.* and Baets & Stein.

a vertical film using optical interferometry. They observed an upward flow in the border close to the film, while a downward flow takes place in the periphery of the border. They attributed this directional influence to surface tension gradients in the film. Stein (1991) described this directional dependence of marginal regeneration as a hydrodynamic instability by taking into account the surface tension gradients in the film that lead to a surface tension-gradient-driven flow, i.e., a Marangoni flow. Stable, vertical liquid films were formed and studied and comparisons were made with corresponding aqueous soap film experiments by Baets & Stein (1994).

More recently, Joye, Hirasaki & Miller (1992, 1994, 1996), studied drainage in circular films and have shown, via a linear stability analysis and numerical simulations, that this hydrodynamic instability is caused by a surface tension-driven (Marangoni) flow. This instability is stabilized by surface viscosity, surface diffusivity and the system length scale. They also argued that the asymmetric drainage seen in their circular films, the behavior observed by Hudales and Stein, and Mysels' theory on marginal regeneration all stem from the hydrodynamic instability described by Stein.

Nierstrasz & Frens (1998, 1999) have also proposed Marangoni effects as a cause for structures observed at the edges of vertical films, they have a computational model of the draining film. Their model is one dimensional, includes a soluble surfactant and seems to be focussed on the region where the film meets the surface of the bath. This is in contrast to our work (Braun, Snow & Pernisz 1999; Naire, Braun & Snow 2000*a*,*b*) where the entire film above this junction and part of the junction area are combined into a single model. Their computations (Nierstrasz & Frens 1999) apparently exhibit jumps of the slope in, and localized spikes in, some of the dependent variables at the junction point (inside the computational domain). They also speculate that the Marangoni effect

may cause instability of the film near the bath leading to the structures at the bottom a vertical draining film.

Snow and co-workers also attributed the surface flows observed at the bottom and the edges of their PU films to surface tension-gradient-driven flows. Their conclusion was based on measurements made for the rate of thinning which were correlated with the drainage rate of the film.

A general consensus that can be arrived at, from all the observations made by the above authors, is that drainage in vertical mobile films is a fine interplay between gravity and surface tension gradients. In the thicker parts of the film, gravity is the dominant effect leading to surface flow in the direction of gravity while at the thinner parts, the surface tension gradient effects dominate, leading to a Marangoni flow opposite to the direction of gravity. It is conjectured that this competition between gravity and the Marangoni effect caused by the redistribution of surfactant along the film surface by the underlying flow is the mechanism driving the instability seen in vertical draining films.

In this paper, we use lubrication theory to derive four nonlinear partial differential equations (PDEs) that describes the time-evolution of the free surface of the fluid interface, surface velocities and the transport of surfactant along the free surface. In previous works by the authors, 1+1 dimensional models have been formulated for both the tangentially-immobile film (Braun *et al.*) and the mobile film (Naire *et al.*). Results from these models will be used as a point of departure for this model. Our endeavour will be to recover some of the experimental structures observed by Snow *et al.*, Baets and Stein, Hudales and Stein, and others. An investigation of the above conjecture as an instability mechanism, by performing a fully nonlinear stability analysis via numerical simulations, is our primary objective in this paper.

The plan of this paper is as follows. In §2, the 2+1 dimensional hydrodynamic problem

is described in both dimensional and nondimensional forms. Lubrication theory is used to arrive at four nonlinear coupled partial differential equations for the evolution of the free surface, the two components of surface velocity and the surfactant concentration on the free surface. Boundary conditions for the PDEs are also prescribed in this section. §3 deals with the numerical scheme that we employ to solve the PDEs. In §4, we examine the 2+1 dimensional tangentially-immobile case which is obtained in the limit of large surface viscosities. This section also discusses some numerical results for this simplified case. In §5, we study the mobile film model. We also show how the tangentially-immobile model can be recovered asymptotically in the limit of large surface shear viscosity. We also present the numerical results for the mobile film problem and explain the instability mechanism observed in the simulations. In §6, comparison is made with the work done by Joye *et al.* §7 summarizes some of the important results and discusses future work.

2. Problem formulation

Consider a 2+1 dimensional draining film in a Cartesian coordinate system $(\bar{x}, \bar{y}, \bar{z})$ (see figure 2). The film is hanging from a thin wire frame at $\bar{z} = 0$ (the $\bar{x}$-$\bar{y}$ plane). Gravity acts in the downward direction so $\mathbf{g} = g\mathbf{k}$, where $\mathbf{k}$ is the unit vector pointing in the positive $\bar{z}$ direction. The free surface of the thin film is given by $\bar{x} = \bar{k}(\bar{y}, \bar{z}, \bar{t})$. The top end of the film is assumed to be fixed at $\bar{k} = k_0$ and the film is assumed to be symmetric about the plane $\bar{x} = 0$. We employ the incompressible Navier–Stokes equation to describe the flow of the bulk liquid. The velocity vector $\bar{\mathbf{v}} = (\bar{u}(\bar{x}, \bar{y}, \bar{z}, \bar{t}), \bar{v}(\bar{x}, \bar{y}, \bar{z}, \bar{t}), \bar{w}(\bar{x}, \bar{y}, \bar{z}, \bar{t}))$ and the pressure $\bar{p}(\bar{x}, \bar{y}, \bar{z}, \bar{t})$ satisfy

$$\bar{\nabla}\cdot\bar{\mathbf{v}} = 0, \tag{2.1}$$

$$\rho\left(\frac{\partial\bar{\mathbf{v}}}{\partial\bar{t}} + \bar{\mathbf{v}}\cdot\bar{\nabla}\bar{\mathbf{v}}\right) = \mu\bar{\nabla}^2\bar{\mathbf{v}} - \bar{\nabla}\bar{p} + \rho g\mathbf{k}, \tag{2.2}$$

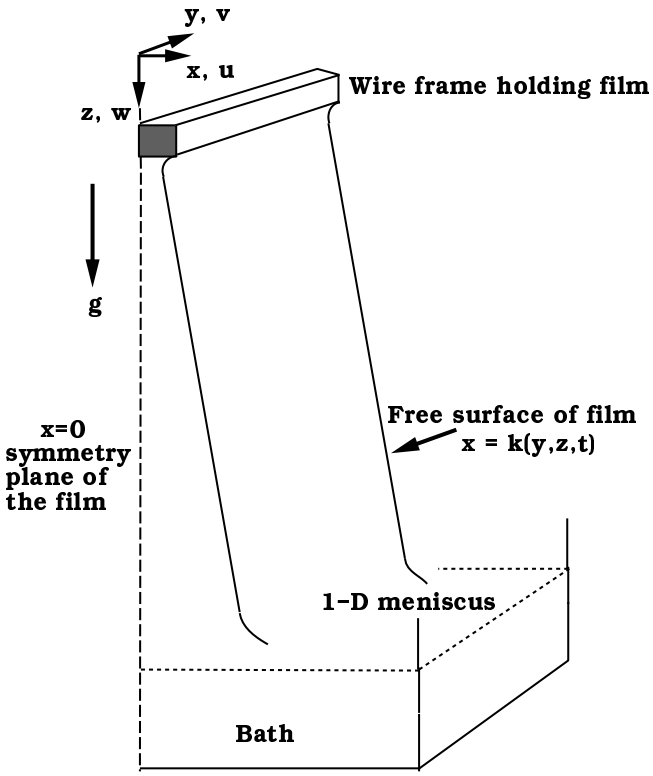

FIGURE 2. 2+1 dimensional schematic representation of the model studied.

where $\mathbf{k} = (0, 0, 1)$, g is the magnitude of gravitational acceleration, ρ is the density and μ is the dynamic shear viscosity of the fluid. We assume ρ and μ to be constant.

Boundary conditions for (2.1) and (2.2) include the symmetry condition at $\bar{x} = 0$ given by

$$\bar{u} = \bar{w}_{\bar{x}} = \bar{v}_{\bar{x}} = 0. \tag{2.3}$$

The instantaneous location of the free surface $\bar{x} = \bar{k}(\bar{y}, \bar{z}, \bar{t})$ is described by the kinematic boundary condition

$$\bar{k}_{\bar{t}} + \bar{\mathbf{v}} \cdot \bar{\nabla} \bar{k} = \bar{u}. \tag{2.4}$$

The normal and the tangential component of the interfacial stress is derived from the Boussinesq-Scriven surface stress model (Boussinesq 1913; Scriven 1960) and is given by

(see Edwards, Brenner & Wasan 1991; Slattery 1990)

$$-\bar{\mathbf{n}}\cdot \parallel \bar{\mathcal{T}} \parallel \cdot\bar{\mathbf{n}} = 2\bar{\mathcal{H}}\bar{\sigma} + 2\bar{\mathcal{H}}(\kappa^{\mathbf{s}} + \mu^{\mathbf{s}})\bar{\nabla}_{\mathbf{s}}\cdot\bar{\mathbf{v}} + 2\mu^{\mathbf{s}}\left(\bar{\mathbf{b}} - 2\bar{\mathcal{H}}\bar{\mathbf{I}}_s\right) : \bar{\nabla}_{\mathbf{s}}\bar{\mathbf{v}}, \tag{2.5}$$

$$\begin{aligned}-\bar{\mathbf{t}}\cdot \parallel \bar{\mathcal{T}} \parallel \cdot\bar{\mathbf{n}} = {} & \bar{\mathbf{t}}\cdot\bar{\nabla}_{\mathbf{s}}\bar{\sigma} + (\kappa^{\mathbf{s}} + \mu^{\mathbf{s}})\bar{\mathbf{t}}\cdot\bar{\nabla}_{\mathbf{s}}\bar{\nabla}_{\mathbf{s}}\cdot\bar{\mathbf{v}} \\ & + \mu^{\mathbf{s}}\bar{\mathbf{t}}\cdot\left[\bar{\mathbf{n}}\times\bar{\nabla}_{\mathbf{s}}\left((\bar{\nabla}_{\mathbf{s}}\times\bar{\mathbf{v}})\cdot\bar{\mathbf{n}}\right)\right] \\ & + 2\mu^{\mathbf{s}}\bar{\mathbf{t}}\left[(\bar{\mathbf{b}} - 2\bar{\mathcal{H}}\bar{\mathbf{I}}_{\mathbf{s}})\cdot\bar{\nabla}_{\mathbf{s}}\bar{\mathbf{v}}\cdot\bar{\mathbf{n}}\right],\end{aligned} \tag{2.6}$$

respectively, for constant surface viscosities. Here, $\bar{\mathbf{n}}$ is the unit outward surface normal and $\bar{\mathbf{t}}$ is the unit tangent vector along the free surface. $\parallel \bar{\mathcal{T}} \parallel = \bar{\mathcal{T}}_{\mathbf{a}} - \bar{\mathcal{T}}$ denotes the jump in the stress tensor across the free surface where $\bar{\mathcal{T}} = -\mathbf{I}\bar{p} + \mu(\bar{\nabla}\bar{\mathbf{v}} + \bar{\nabla}\bar{\mathbf{v}}^{t})$ is the stress tensor and $\bar{\mathcal{T}}_{\mathbf{a}}$ is the stress tensor in the outside air phase (assumed to be zero). $\bar{\mathcal{H}}$ is the mean curvature of the free surface, $\bar{\sigma}$ is the surface tension, $\kappa^{\mathbf{s}}$ and $\mu^{\mathbf{s}}$ are the surface dilatational and shear viscosity coefficients, respectively, $\bar{\nabla}_{\mathbf{s}}$ denotes the surface gradient operator, $\bar{\mathbf{b}} = -\bar{\nabla}_{\mathbf{s}}\bar{\mathbf{n}}$ is the surface curvature dyadic and $\bar{\mathbf{I}}_{\mathbf{s}} = \mathbf{I} - \bar{\mathbf{n}}\bar{\mathbf{n}}$ is the spatial idemfactor. Surface differentiation operators are based on Scriven, Stone (1990) and Wong, Rumschitzki & Maldarelli (1996).

For the case when the fluid surface contains a dilute insoluble surfactant, surface tension is no longer a constant and is assumed to behave according to

$$\sigma(\bar{\Gamma}) = \bar{\sigma}_m - \left(\frac{\partial\bar{\sigma}}{\partial\bar{\Gamma}}\right)_{\bar{\Gamma}_m}\left(\bar{\Gamma} - \bar{\Gamma}_m\right), \tag{2.7}$$

where $\bar{\sigma}_m = \sigma(\bar{\Gamma}_m)$. We will typically assume that $\bar{\Gamma}_m$ is a reference concentration.

The transport equation for the surfactant on the free surface is (Scriven; Stone; and Wong *et al.*).

$$\frac{\partial\bar{\Gamma}}{\partial\bar{t}} + \bar{\nabla}_s\cdot(\bar{\Gamma}\bar{\mathbf{v}}) = \mathcal{D}_s\bar{\nabla}_s^2\bar{\Gamma} - \bar{\mathbf{n}}\cdot\mathbf{j}, \tag{2.8}$$

where the surface concentration of surfactant is $\bar{\Gamma} = \bar{\Gamma}\left(\bar{k}(\bar{y},\bar{z},\bar{t}),\bar{y},\bar{z},\bar{t}\right)$ and $\mathcal{D}_s$ is the

surface diffusivity. Here, $-\bar{\mathbf{n}}\cdot\mathbf{j}$ is the flux of the surfactant between the bulk and the free surface, for the insoluble case, $\mathbf{j} = \mathbf{0}$.

2.1. *Nondimensionalization*

We will use length scales based on the tangentially-immobile case (Wilson 1982; Braun *et al.* 1999; Naire *et al.* 2000*a*,*b*) The three length scales are

$$d = \sqrt{\frac{\mu W}{\rho g}}, \qquad D = \sqrt{\frac{\bar{\sigma}}{\rho g}} \qquad \text{and} \qquad \ell = d^{1/3}D^{2/3}; \tag{2.9}$$

they are the film thickness d, equilibrium meniscus radius D, and the intermediate scale ℓ, respectively. Using an experimentally determined value for d, the corresponding vertical velocity scale is given by solving for W. Separation of scales occurs with

$$\delta^2 = \frac{d}{\ell} \ll 1. \tag{2.10}$$

We then introduce the following nondimensionalizations

$$x = \frac{\bar{x}}{d}, \quad y = \frac{\bar{y}}{\ell}, \quad z = \frac{\bar{z}}{\ell}, \quad t = \frac{W}{\ell}\bar{t}, \quad u = \frac{\bar{u}}{\delta^2 W}, \tag{2.11}$$
$$v = \frac{\bar{v}}{W}, \quad w = \frac{\bar{w}}{W}, \quad p = \frac{\delta^4\ell}{\mu W}\bar{p}, \quad \Gamma = \frac{\bar{\Gamma}}{\bar{\Gamma}_m} \quad \text{and} \quad \sigma = \frac{\bar{\sigma}}{\bar{\sigma}_m}.$$

Substituting the dimensionless variables into the equations governing the flow inside the film ((2.1) and (2.2)) furnishes the following dimensionless problem. Inside the film, we have

$$u_x + v_y + w_z = 0, \tag{2.12}$$

$$\delta^8\mathrm{Re}(u_t + uu_x + vu_y + wu_z) = \delta^4(u_{xx} + \delta^8 u_{yy} + \delta^8 u_{zz}) - p_x, \tag{2.13}$$

$$\delta^4\mathrm{Re}(v_t + uv_x + vv_y + wv_z) = v_{xx} + \delta^4(v_{yy} + v_{zz}) - p_y, \tag{2.14}$$

$$\delta^4\mathrm{Re}(w_t + uw_x + vw_y + ww_z) = w_{xx} + \delta^4(w_{yy} + w_{zz}) - p_z + 1. \tag{2.15}$$

On the plane $x = 0$ (the y-z plane), symmetry requires $u = v_x = w_x = 0$. The kinematic

condition becomes

$$k_t - u + k_y v + k_z w = 0. \tag{2.16}$$

The tangential and normal components of the interfacial stress condition can be written as

$$\begin{aligned}\mathcal{T}_{t_i}^{(b)} &= -\mathcal{M}\mathbf{t}_i\cdot\nabla_{\mathbf{s}}\Gamma + \mathcal{S}\mathbf{t}_i\cdot\nabla_{\mathbf{s}}\nabla_{\mathbf{s}}\cdot\mathbf{v} + \bar{\mathcal{S}}\mathbf{t}_i\cdot\Big\{\mathbf{n}\times\nabla_{\mathbf{s}}\left[(\nabla_{\mathbf{s}}\times\mathbf{v})\cdot\mathbf{n}\right] \\ &\quad + 2(\mathbf{b} - 2\delta^2\mathcal{H}\mathbf{I}_{\mathbf{s}})\cdot\nabla_{\mathbf{s}}\mathbf{v}\cdot\mathbf{n}\Big\}, \end{aligned}\tag{2.17}$$

$$\begin{aligned}\mathcal{T}_{n}^{(b)} &= 2\mathcal{H}\left[1 - \delta^4\mathcal{M}(\Gamma - 1)\right] + 2\mathcal{S}\delta^4\mathcal{H}\nabla_{\mathbf{s}}\cdot\mathbf{v} \\ &\quad + 2\bar{\mathcal{S}}\delta^2\left(\mathbf{b} - 2\delta^2\mathcal{H}\mathbf{I}_s\right) : \nabla_{\mathbf{s}}\mathbf{v}, \end{aligned}\tag{2.18}$$

respectively. Here,

$$\begin{aligned}\mathcal{T}_{t_1}^{(b)} &= N\left[2\delta^4 k_y(u_x - v_y) + (\delta^4 u_y + v_x)(1 - \delta^4 k_y^2) - \delta^4 k_y k_z(\delta^4 u_z + w_x)\right. \\ &\quad \left. -\delta^4 k_z(v_z + w_y)\right], \end{aligned}\tag{2.19}$$

$$\begin{aligned}\mathcal{T}_{t_2}^{(b)} &= -N^2\Big\{2\delta^4 k_z u_x + 2\delta^8 k_y^2 k_z v_y - 2\delta^4 k_z(1 + \delta^4 k_y^2)w_z - 2\delta^4 k_y k_z(\delta^4 u_y + v_x) \\ &\quad + (\delta^4 u_z + w_x)(1 + \delta^4 k_y^2 - \delta^4 k_z^2) \\ &\quad + (v_z + w_y)\left[\delta^8 k_y k_z^2 - \delta^4 k_y(1 + \delta^4 k_y^2)\right]\Big\}, \end{aligned}\tag{2.20}$$

$$\begin{aligned}\mathcal{T}_{n}^{(b)} &= -p + 2\delta^4 N^2\left[u_x + k_y(\delta^4 k_y v_y - \delta^4 u_y - v_x) + k_z(\delta^4 k_z w_z - \delta^4 u_z - w_x)\right. \\ &\quad \left. +\delta^4 k_y k_z(v_z + w_y)\right], \end{aligned}\tag{2.21}$$

are the two tangential and normal stress components due to the bulk viscous stresses, respectively, and

$$N := \frac{1}{\sqrt{1 + \delta^4 k_y^2 + \delta^4 k_z^2}}. \tag{2.22}$$

On the free surface of the plane we have a nondimensional surfactant transport equation given by

$$\frac{\partial\Gamma}{\partial t} + \nabla_s\cdot(\Gamma\mathbf{v}) = \frac{1}{Pe}\nabla_s{}^2\Gamma, \tag{2.23}$$

Number	Definition	Comparison of forces
Reynolds	$\mathrm{Re} = \frac{\rho W \ell}{\mu}$	$\frac{\text{inertial}}{\text{viscous shear}}$
Modified Boussinesq	$\mathcal{S} = \frac{(\kappa^s + \mu^s)_m W/\ell^2}{\mu W/d}$	$\frac{\text{surface viscous}}{\text{viscous shear}}$
	$\bar{\mathcal{S}} = \frac{\mu^s_m W/\ell^2}{\mu W/d}$	$\frac{\text{surface viscous shear}}{\text{viscous shear}}$
Capillary	$\mathcal{C} = \frac{\mu W}{\bar{\sigma}_m}$	$\frac{\text{viscous shear}}{\text{surface tension}}$
Marangoni	$\mathcal{M} = \frac{\bar{\Gamma}_m \left(\frac{\partial \bar{\sigma}}{\partial \bar{\Gamma}}\right)_{\bar{\Gamma}_m}}{\mu W} \delta^2$	$\frac{\text{concentration gradient shear}}{\text{viscous shear}}$
Péclet	$Pe = \frac{W\ell}{\mathcal{D}_s}$	$\frac{\text{advective transport}}{\text{diffusive transport}}$

TABLE 1. Table of nondimensional parameters and their interpretations.

Note that in our scalings $\mathcal{C} = \delta^6$ (see Naire *et al.*).

Several dimensionless groups have appeared and they are listed in table 1.

2.2. *Lubrication Theory*

We seek solutions in the form of a regular perturbation expansion in powers of δ^4:

$$(u, v, w, k, p, \Gamma) = (u, v, w, k, p, \Gamma)^{(0)} + \delta^4 (u, v, w, k, p, \Gamma)^{(1)} + \ldots \tag{2.24}$$

Substituting the series expansions into the scaled equations and dropping superscripts gives to leading order in the bulk (inside the film)

$$u_x + v_y + w_z = 0, \tag{2.25}$$

$$0 = -p_x, \tag{2.26}$$

$$0 = v_{xx} - p_y \tag{2.27}$$

$$0 = w_{xx} - p_z + 1. \tag{2.28}$$

These are subject to the symmetry condition at $x = 0$ ($y - z$ plane),

$$u = v_x = w_x = 0. \tag{2.29}$$

At $x = k(y,z,t)$ we have

$$\kappa = -p, \tag{2.30}$$

$$-N\mathcal{M}\Gamma_y + \mathcal{S}N\mathcal{A}_2(N^2\mathcal{A}_2 v + N^2\mathcal{A}_3 w) - \bar{\mathcal{S}}N^3\mathcal{A}_3(N^2\mathcal{A}_2 w - N^2\mathcal{A}_3 v) = v_x, \tag{2.31}$$

$$-N\mathcal{M}\Gamma_z + \mathcal{S}N\mathcal{A}_3(N^2\mathcal{A}_2 v + N^2\mathcal{A}_3 w) + \bar{\mathcal{S}}N^3\mathcal{A}_2(N^2\mathcal{A}_2 w - N^2\mathcal{A}_3 v) = w_x, \tag{2.32}$$

$$k_t - u + k_y v + k_z w = 0, \tag{2.33}$$

where

$$\kappa = N^3(k_{yy} + k_{zz}) = \frac{k_{yy} + k_{zz}}{\left[1 + \delta^4(k_y^2 + k_z^2)\right]^{3/2}}, \tag{2.34}$$

is the full curvature of the film and

$$\mathcal{A}_2 := k_y \frac{\partial}{\partial x} + \frac{\partial}{\partial y}, \tag{2.35}$$

$$\mathcal{A}_3 := k_z \frac{\partial}{\partial x} + \frac{\partial}{\partial z}. \tag{2.36}$$

This model relies on results from previous work by Kheshgi, Kistler & Scriven (1992) and Ruschak (1978), who have shown that it is possible to keep the full curvature in the normal stress condition and integrate through the matching region onto the static meniscus.

Using (2.27), (2.28) (2.30) and symmetry at $x = 0$ we obtain

$$v = -\kappa_y \frac{x^2}{2} + B_v(y,z,t), \tag{2.37}$$

$$w = -(1 + \kappa_z)\frac{x^2}{2} + B_w(y,z,t). \tag{2.38}$$

We define

$$v^{(S)}(y,z,t) := -\kappa_y \frac{k^2}{2} + B_v(y,z,t), \tag{2.39}$$

$$w^{(S)}(y,z,t) := -(1 + \kappa_z)\frac{k^2}{2} + B_w(y,z,t); \tag{2.40}$$

where $v^{(S)}$ and $w^{(S)}$ are the surface velocities in the y and z directions respectively. (2.31)

and (2.32), become

$$\mathcal{S}N^2(v_{yy}^{(S)} + w_{yz}^{(S)}) - \bar{\mathcal{S}}N^2(w_{yz}^{(S)} - v_{zz}^{(S)}) + Nk\kappa_y - \mathcal{M}\Gamma_y = 0, \tag{2.41}$$

$$\mathcal{S}N^2(v_{yz}^{(S)} + w_{zz}^{(S)}) + \bar{\mathcal{S}}N^2(w_{yy}^{(S)} - v_{zy}^{(S)}) + Nk(\kappa_z + 1) - \mathcal{M}\Gamma_z = 0. \tag{2.42}$$

From the kinematic condition we obtain

$$k_t + \nabla_{\mathrm{II}}\cdot\left(k\mathbf{v}^{(S)} + \frac{k^3}{3}\nabla_{\mathrm{II}}\kappa\right) + \left(\frac{k^3}{3}\right)_z = 0, \tag{2.43}$$

where

$$\nabla_{\mathrm{II}} := \left(\frac{\partial}{\partial y}, \frac{\partial}{\partial z}\right) \quad \text{and} \quad \mathbf{v}^{(S)} := \left(v^{(S)}, w^{(S)}\right). \tag{2.44}$$

This evolution equation is coupled with the equations for the surface velocities, (2.41) and (2.42), and the equation for surfactant transport given by

$$\Gamma_t + N^2\nabla_{\mathrm{II}}\cdot\left[\Gamma\mathbf{v}^{(S)} - \frac{1}{Pe}N^2\nabla_{\mathrm{II}}\Gamma\right] = 0. \tag{2.45}$$

(2.41), (2.42), (2.43) and (2.45) have all the ingredients that include the effects of curvature, gravity, surface viscosity, the Marangoni effect, convective and diffusive surfactant transport.

We have retained some normalization factors, i.e., powers of N, in (2.41), (2.42) and (2.45); this is done so as to be consistent with keeping the full curvature term. For a standard lubrication analysis, N would normally be unity at leading order; the equations could then be simplified to

$$k_t + \nabla_{\mathrm{II}}\cdot\left(k\mathbf{v}^{(S)} + \frac{k^3}{3}\nabla_{\mathrm{II}}\kappa\right) + \left(\frac{k^3}{3}\right)_z = 0, \tag{2.46}$$

$$\mathcal{S}(v_{yy}^{(S)} + w_{yz}^{(S)}) - \bar{\mathcal{S}}(w_{yz}^{(S)} - v_{zz}^{(S)}) + k\kappa_y - \mathcal{M}\Gamma_y = 0, \tag{2.47}$$

$$\mathcal{S}(v_{yz}^{(S)} + w_{zz}^{(S)}) + \bar{\mathcal{S}}(w_{yy}^{(S)} - v_{zy}^{(S)}) + k(\kappa_z + 1) - \mathcal{M}\Gamma_z = 0, \tag{2.48}$$

$$\Gamma_t + \nabla_{\mathrm{II}}\cdot\left[\Gamma\mathbf{v}^{(S)} - \frac{1}{Pe}\nabla_{\mathrm{II}}\Gamma\right] = 0. \tag{2.49}$$

Similar forms of the above film equations has appeared in the literature (see Edwards & Oron 1995; Ida & Miksis 1998*a*,*b*).

By incorporating surface viscous effects into our model we have a set of nonlinear coupled partial differential equations at leading order that fully describe the evolution of the free surface, the surface velocities and the concentration of surfactant along the free surface. By the definition of the surface velocities, $v^{(S)}(y,z,t)$and $w^{(S)}(y,z,t)$, we have introduced natural variables into our model; this is preferred over the unknowns $B_v(y,z,t)$ and $B_w(y,z,t)$, because we would get fifth order derivatives of k if these latter unknowns are kept. Such higher order derivatives would make our computations and analysis to follow much more difficult.

2.3. *Boundary conditions*

Boundary conditions for (2.41), (2.42), (2.43) and (2.45) are specified as follows (see figure 3).

The system is assumed to be symmetric at the transverse boundaries in the y direction; we consider this instead of periodic boundary conditions for computational convenience. This means that there is no flux normal to the y boundaries ($y = 0$ and $y = L_y$), where L_y is the length of the computational domain in the y direction. Similarly, there is no surfactant flux normal to these boundaries. We thus have

$$k_y = k_{yyy} = \Gamma_y = v^{(S)} = w_y^{(S)} = 0 \quad \text{at} \quad y = 0 \quad \text{and} \quad y = L_y, \quad 0 \le z \le L_z. \quad (2.50)$$

The above two boundary conditions for $v^{(S)}$ and $w^{(S)}$ essentially mean that there is no flow out of the y boundaries and no shear along the y boundaries, respectively.

At $z = 0$, the film is pinned to the wire frame and there is no flux out of the frame. Also, we have no surfactant flux out of the wire frame. Hence

$$k = 1, \quad \kappa_z = -1, \quad v^{(S)} = w^{(S)} = 0 \quad \text{and} \quad \Gamma_z = 0 \quad \text{at} \quad z = 0, \quad 0 \le y \le L_y. \quad (2.51)$$

At the bottom, i.e., $z = L_z$, we assume that the film connects onto a one dimensional static meniscus. The virtually static meniscus below is governed by the Young Laplace equation, i.e.,

$$\kappa_z = -1. \tag{2.52}$$

Solutions of the Young Laplace equation for two-dimensional menisci are parametrized by α,

$$\frac{\alpha}{\delta^2} = \kappa^2 + \frac{2k_z}{\sqrt{1+\delta^4 k_z^2}}, \tag{2.53}$$

a constant in the first integral of (2.52): for an infinite bath at the bottom of the film, we have $\alpha = 2$. If we think of specifying a boundary condition where we fix k_z, we may then use (2.53) to specify k_{zz} for an infinite bath, via

$$k_{zz} = \sqrt{2\left(\frac{1}{\delta^2} - \frac{k_z}{\sqrt{1+\delta^4 k_z^2}}\right)(1+\delta^4 k_z^2)^3}. \tag{2.54}$$

We specify α and k_z at the bottom of the film, and k_{zz} is then known (Kheshgi *et al.* and Ruschak);

$$k_z = s_0, \quad k_{zz} = s_1 \quad \text{at} \quad z = L_z, \quad 0 \le y \le L_y. \tag{2.55}$$

For a specified slope, s_0, we can compute the corresponding curvature, s_1, using (2.54).

We also need the following boundary conditions for $v^{(S)}$, $w^{(S)}$ and Γ to get the right behavior so as to connect onto the meniscus.

$$\Gamma_z = v^{(S)} = w^{(S)} = 0 \quad \text{at} \quad z = L_z, \quad 0 \le y \le L_y. \tag{2.56}$$

These are the complete boundary conditions for the film problem.

3. Numerical scheme

The spatial derivatives involved in (2.41)-(2.43) and (2.45) are approximated by appropriate second order accurate finite difference approximations keeping the time derivative

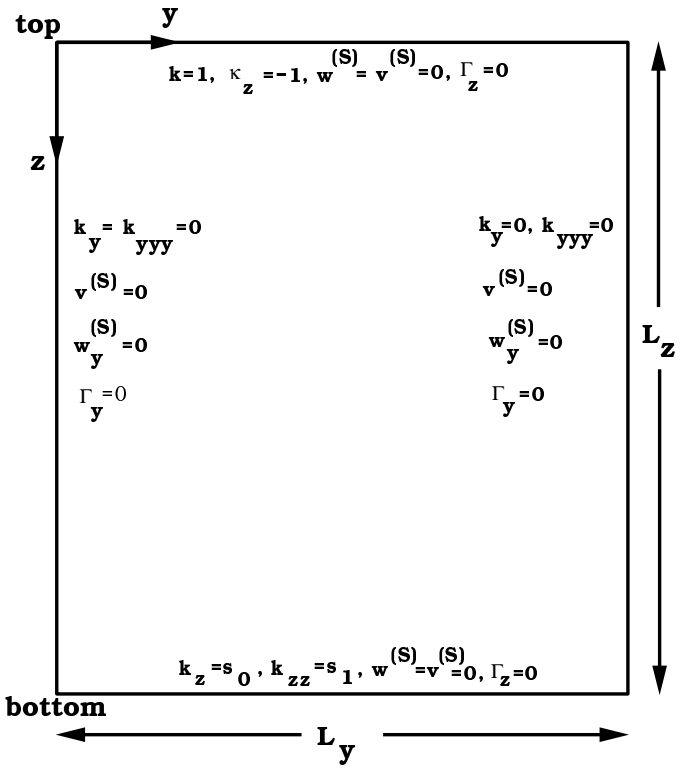

FIGURE 3. Boundary conditions for film model.

continuous. The resulting equations can be written in the form of a system of differential-algebraic equations, or DAEs (Brennan, Campbell & Petzold 1996); to solve them we have used the package DASPK (Li & Petzold 1999). The solution procedure and some of the features of this package will be explained in what follows.

Writing (2.43) in terms of the fluxes in the y and z direction we obtain

$$k_t + \mathcal{Q}_y^{(y)} + \mathcal{Q}_z^{(z)} = 0, \tag{3.1}$$

where

$$\mathcal{Q}^{(y)} := kv^{(S)} + \frac{k^3}{3}\left[\frac{k_{yy}+k_{zz}}{\sqrt{1+\delta^4(k_y^2+k_z^2)}}\right]_y \quad \text{and} \tag{3.2}$$

$$\mathcal{Q}^{(z)} := kw^{(S)} + \frac{k^3}{3}\left[\left(\frac{k_{yy}+k_{zz}}{\sqrt{1+\delta^4(k_y^2+k_z^2)}}\right)_z + 1\right], \tag{3.3}$$

are fluxes in the y and z direction, respectively. This evolution equation is coupled with

$$\mathcal{S}N^2(v_{yy}^{(S)} + w_{yz}^{(S)}) - \bar{\mathcal{S}}N^2(w_{yz}^{(S)} - v_{zz}^{(S)}) + Nk\kappa_y - \mathcal{M}\Gamma_y = 0, \tag{3.4}$$

$$\mathcal{S}N^2(v_{yz}^{(S)} + w_{zz}^{(S)}) + \bar{\mathcal{S}}N^2(w_{yy}^{(S)} - v_{zy}^{(S)}) + Nk(\kappa_z + 1) - \mathcal{M}\Gamma_z = 0, \tag{3.5}$$

$$\Gamma_t + N^2(\mathcal{Q}_y^{(s,y)} + \mathcal{Q}_z^{(s,z)}) = 0, \tag{3.6}$$

where

$$\mathcal{Q}^{(s,y)} := \Gamma v^{(S)} + \frac{N^2}{Pe}\Gamma_y, \tag{3.7}$$

$$\mathcal{Q}^{(s,z)} := \Gamma w^{(S)} + \frac{N^2}{Pe}\Gamma_z, \tag{3.8}$$

are the surfactant fluxes in the y and z direction, respectively. Writing the evolution and the surfactant transport equations in this form ensures conservation of the fluxes over the film region and our numerical method has to preserve this conservation property regardless of accuracy.

The spatial derivatives involved are then approximated by finite difference approximations with the time derivative kept continuous. In order to do this, the dependent variables, k, $v^{(S)}$, $w^{(S)}$ and Γ are evaluated on discrete grid points $y_i = i\Delta y$ and $z_j = j\Delta z$ where $0 \le i \le N$ and $0 \le j \le M$; we then have $k_{i,j} = k(y_i, z_j, t)$, $v_{i,j}^{(S)} = v^{(S)}(y_i, z_j, t)$, $w_{i,j}^{(S)} = w^{(S)}(y_i, z_j, t)$ and $\Gamma_{i,j} = \Gamma(y_i, z_j, t)$. Here $\Delta y = L_y/N$ and $\Delta z = L_z/M$ where L_y and L_z are the lengths of the computational domain in the y and z directions, respectively. We use a staggered numbering system to order the unknowns, i.e., the unknowns are considered in the order of

$$\left[(k_{i,j}, v_{i,j}^{(S)}, w_{i,j}^{(S)}, \Gamma_{i,j}), j = 0, \ldots, M\right], i = 0, \ldots, N \tag{3.9}$$

This ordering greatly reduces the bandwidth of the system and storage requirements compared with say an ordering such as:

$$(k_{i,j}, j = 1, \ldots, M), i = 0, \ldots, N; (v_{i,j}^{(S)}, j = 1, \ldots, M), i = 0, \ldots, N;$$

$$(w_{i,j}^{(S)}, j = 1, \ldots, M), i = 0, \ldots, N; (\Gamma_{i,j}, j = 1, \ldots, M), i = 0, \ldots, N. \tag{3.10}$$

The resulting differential-algebraic system derived after spatial discretization can be written as

$$\mathcal{G}(t, y, y') = 0, \tag{3.11}$$

where

$$y(t) := [y_1, y_2, \ldots, y_N], \quad y'(t) := [y_1', y_2', \ldots, y_N'] \quad \text{and} \quad ' := \frac{d}{dt}. \tag{3.12}$$

N is the total number of unknowns in the system and the y_i's could be either differential or algebraic variables. We use DASPK to solve (3.11).

DASPK uses backward differentiation formula (BDF) methods (Petzold *et al.*) in time to solve the system of DAEs. The methods are variable step-size and variable order. The system of equations is written in implicit form as in (3.11); following discretization in t by BDF methods, a nonlinear equation

$$\mathcal{G}(t^m, y_i^m, \alpha y_i^m + \beta) = 0, \tag{3.13}$$

must be solved at each time step, t^m (current time step), where $\alpha = \alpha_0/h^m$ is a constant which changes whenever the stepsize or order changes, β is a vector which depends on the solution at past times.

DASPK solves (3.13) by a modified version of Newton's method

$$y^{m+1} = y^m - c\left(\alpha \frac{\partial \mathcal{G}}{\partial y_t} + \frac{\partial \mathcal{G}}{\partial y}\right)^{-1} \mathcal{G}(t, y^m, \alpha y^m + \beta). \tag{3.14}$$

The linear system is solved by using the preconditioned GMRES (Generalized Minimum Residual) iterative method (e.g., Kelly 1995; Saad 1996) at each Newton iteration. Several preconditioners have been used; one of them is the incomplete LU factorization (ILU) preconditioner, which can be used for any sparse linear system.

One of the difficulties in using DASPK is that the integration must be started with a

consistent set of initial conditions for all the dependent variables and their time derivatives. This means that we need consistent initial conditions for the algebraic variables which in our case are $v^{(S)}$ and $w^{(S)}$. For the case when $\mathcal{S}$=$\bar{\mathcal{S}}$, i.e., zero dilatational viscosity, (2.41) and (2.42) reduce to the familiar Poisson equation, for a given initial k and Γ. We can use any standard Poisson solver to get the corresponding consistent $v^{(S)}$ and $w^{(S)}$. It is for the general and physically interesting case when $\mathcal{S} \neq \bar{\mathcal{S}}$, i.e., non-zero dilatational viscosity, that a consistent $v^{(S)}$ and $w^{(S)}$ is more difficult to compute.

4. Tangentially-immobile film

(2.41), (2.42), (2.43) and (2.45), are a strongly coupled nonlinear mixed system of parabolic and elliptic PDEs with a number of nondimensional parameters. This poses a very challenging problem not only in understanding the physics of the problem but also in the numerical implementation of it. A first step towards understanding the full problem is to consider a limiting case. Thus, we will first consider the tangentially-immobile problem (see Braun *et al.*, for the 1+1 dimensional tangentially immobile case). The surface is assumed to be packed with surfactant; then Γ is assumed constant, and the large value makes the surface tangentially-immobile, i.e., $v^{(S)} = w^{(S)} = 0$. Mathematically, this surface can be realized in the limit of $\mathcal{S} = \bar{\mathcal{S}} \to \infty$; this is discussed in more detail in §5.1. The governing equation for the tangentially-immobile model is then given by

$$k_t + \nabla_{\mathrm{II}} \cdot \left(\frac{k^3}{3} \nabla_{\mathrm{II}} \kappa \right) + \left(\frac{k^3}{3} \right)_z = 0, \tag{4.1}$$

The assumption of a rigid surface has enabled us to greatly simplify the problem from three coupled nonlinear equations to just one parabolic PDE for the evolution of the free surface $x = k(y, z, t)$.

Our goal is to see whether the film is stable to tranverse perturbations, i.e., perturbations in the y direction. A linear stability analysis cannot be done analytically because

this problem has no steady state solution about which a perturbation could be imposed. Hence, we have to resort to numerical computations to perform a full nonlinear stability analysis. This is discussed in the next section.

4.1. *Numerical results*

As described in §3, to solve (4.1), we have used a second order accurate finite difference scheme to discretize the spatial derivatives leaving the time derivative continuous. The resulting equations are in the form of a differential-algebraic system; to solve them we have used the package DASPK (Li & Petzold). Our main goal in this numerical experiment is to see whether the system is stable to transverse perturbations, i.e., perturbations along the y direction. We attempt a full nonlinear stability analysis numerically; we will introduce a perturbation via the initial condition $k(y,z,0)$ and see whether these perturbations grow or decay in time. These perturbations will be concentrated near the bottom where the film is close to the bath. From the 1+1 dimensional calculations, Braun *et al.*, have observed that there is a sequence of bumps and dips near the bottom as the film enters the bath; we believe that stability of these bumps and dips may be important in explaining observed patterns.

For the results to follow, we consider an initial shape

$$k(y,z,0) = \begin{cases} 1 + \mathcal{D}z\cos(\frac{6\pi y}{L_y}), & 0 \le z \le z_1. \\ 1 + r_s - \sqrt{r_s - (z-z_1)^2}, & z_1 < z \le L_z. \end{cases} \tag{4.2}$$

where $\mathcal{D} = 0.05$, the length of the computational box in the y and z directions are given by $L_y = L_z = 37.5$, respectively and $z_1 = 36.504962$, can be thought of as the z location where the film enters the bath. The equation of the static meniscus is given by

$$r_s = \sqrt{1+s_0^2}\left(\frac{L_z - z_1}{s_0}\right), \tag{4.3}$$

where $s_0 = 10$ is the slope at the bottom of the film. The value of $\delta = 0.1$ (fixed from

experiment). We have used a 200 × 80 grid as our finite difference mesh, i.e., 200 points in the z direction and 80 in the y direction. All computations have been done in parallel on a SGI Origin 2000 workstation with 4 300-MHz IP27 processors.

Figure 4 plots the free surface shape k at time $t = 2$. The perturbations near the bottom of the film are still almost the same magnitude as the initial shape. We clearly see the four distinct film regimes, i.e., meniscus forming at the top, long, flat middle region connecting to the static meniscus via a transition region consisting of bumps and dips whose amplitude diminishes rapidly up the film. This is consistent with our observation from the 1+1dimensional computations (Braun *et al.* 1999). The one dimensional static meniscus approximation does not work very well for early times. Figure 5 plots k at time $t = 6$. The perturbations near the bottom are slowly decaying, the one dimensional static meniscus approximation is still not good. Figure 6 plots k at time $t = 16$. The perturbations near the bottom are now decaying rapidly. The film takes on a concave-in shape consistent with the 1+1 dimensional computations (Braun *et al.* 1999); the one dimensional meniscus approximation is thus getting much better. Figure 7 plots k at time $t = 45$. The perturbations have all decayed and the film is uniformly thinning rapidly. The one dimensional static meniscus approximation is now very good.

Hence as time increases, we observe that the bumps near the bottom quickly decay and the film thins uniformly in y; the one dimensional static meniscus approximation therefore improves. This is what we had expected to see considering the fact that the tangentially-immobile model is a limiting case when $\bar{\mathcal{S}}$ (surface shear viscosity) $\rightarrow \infty$; these large surface viscosities act as stabilizing factors due to their energy dissipating effect.

5. Mobile film

The equations governing the mobile film are given by

$$k_t + \nabla_{\mathbf{II}} \cdot \left(k\mathbf{v}^{(S)} + \frac{k^3}{3} \nabla_{\mathbf{II}} \kappa \right) + \left(\frac{k^3}{3} \right)_z = 0, \tag{5.1}$$

$$\mathcal{S}N^2(v_{yy}^{(S)} + w_{yz}^{(S)}) - \bar{\mathcal{S}}N^2(w_{yz}^{(S)} - v_{zz}^{(S)}) + Nk\kappa_y - \mathcal{M}\Gamma_y = 0, \tag{5.2}$$

$$\mathcal{S}N^2(v_{yz}^{(S)} + w_{zz}^{(S)}) + \bar{\mathcal{S}}N^2(w_{yy}^{(S)} - v_{zy}^{(S)}) + Nk(\kappa_z + 1) - \mathcal{M}\Gamma_z = 0, \tag{5.3}$$

$$\Gamma_t + \nabla_{\mathbf{II}} \cdot \left[\Gamma \mathbf{v}^{(S)} - \frac{1}{Pe} \nabla_{\mathbf{II}} \Gamma \right] = 0. \tag{5.4}$$

(5.1) and (5.4) are parabolic equations and equations (5.2) and (5.3) are elliptic.

We have now a more complex problem at hand with four coupled nonlinear mixed type of PDEs. For the case when $\mathcal{S}$=$\bar{\mathcal{S}}$, (5.2) and (5.3) reduce to a Poisson-type equation. The physically interesting case (as we shall see later on in the numerical results) is when $\mathcal{S}$ $\neq$ $\bar{\mathcal{S}}$. (5.2) and (5.3) take on a more general elliptic form for this case and the numerics prove to be challenging.

In the next section, we will attempt to recover asymptotically the tangentially-immobile case from the mobile film equations in the limit of large $\bar{\mathcal{S}}$.

5.1. *Large $\bar{\mathcal{S}}$ asymptotics*

In this section, we will show mathematically how to recover the previously discussed tangentially-immobile model as $\bar{\mathcal{S}}$ (surface shear viscosity) becomes large. Note that $\mathcal{S} \geq \bar{\mathcal{S}}$; this implies that $\mathcal{S} \to \infty$ whenever $\bar{\mathcal{S}} \to \infty$. Thus, without loss of generality, we can consider the case when $\bar{\mathcal{S}} = \mathcal{S}$ is large. (5.1), (5.2), (5.3) and (5.4), for the case when $\mathcal{S} = \bar{\mathcal{S}}$, can be simplified to

$$k_t + \nabla_{\mathbf{II}} \cdot \left(k\mathbf{v}^{(S)} + \frac{k^3}{3} \nabla_{\mathbf{II}} \kappa \right) + \left(\frac{k^3}{3} \right)_z = 0, \tag{5.5}$$

$$v_{yy}^{(S)} + v_{zz}^{(S)} + \frac{1}{\bar{\mathcal{S}}N} k\kappa_y - \frac{1}{\bar{\mathcal{S}}N^2} \mathcal{M}\Gamma_y = 0, \tag{5.6}$$

$$w_{yy}^{(S)} + w_{zz}^{(S)} + \frac{1}{\bar{\mathcal{S}}N} k(\kappa_z + 1) - \frac{1}{\bar{\mathcal{S}}N^2} \mathcal{M}\Gamma_z = 0, \tag{5.7}$$

$$\Gamma_t + \nabla_{\mathbf{II}} \cdot \left[\Gamma \mathbf{v}^{(S)} - \frac{1}{Pe} \nabla_{\mathbf{II}} \Gamma \right] = 0. \tag{5.8}$$

When $\bar{\mathcal{S}} \gg 1$, we can write the solutions as a regular perturbation expansion in powers of $1/\bar{\mathcal{S}}$, i.e.,

$$(k, v^{(S)}, w^{(S)}, \Gamma) = (k, v^{(S)}, w^{(S)}, \Gamma)^{(0)} + \frac{1}{\bar{\mathcal{S}}} (k, v^{(S)}, w^{(S)}, \Gamma)^{(1)} + \ldots \tag{5.9}$$

We assume that $Pe = O(\bar{\mathcal{S}})$; hence diffusion of surfactant will be neglected in the following leading order analysis.

The $O(1)$ problem is

$$k_t^{(0)} + \nabla_{\mathbf{II}} \cdot \left(k^{(0)} \mathbf{v}^{(S,0)} + \frac{{k^{(0)}}^3}{3} \nabla_{\mathbf{II}} \kappa^{(0)} \right) + \left(\frac{{k^{(0)}}^3}{3} \right)_z = 0, \tag{5.10}$$

$$v_{yy}^{(S,0)} + v_{zz}^{(S,0)} = 0, \tag{5.11}$$

$$w_{yy}^{(S,0)} + w_{zz}^{(S,0)} = 0, \tag{5.12}$$

$$\Gamma_t^{(0)} + \nabla_{\mathbf{II}} \cdot \left[\Gamma^{(0)} \mathbf{v}^{(S,0)} \right] = 0. \tag{5.13}$$

$v^{(S,0)}$ satisfies the Laplace equation with zero Dirichlet boundary conditions, this implies that $v^{(S,0)} = 0$. $w^{(S,0)}$ also satisfies the Laplace equation with zero Dirichlet boundary conditions at $z = 0, L_z$ and zero Neumann boundary conditions at $y = 0, L_y$; using a standard separation of variables argument, we obtain $w^{(S,0)} = 0$. Hence, the leading order surface velocity, i.e.,

$$\mathbf{v}^{(S,0)} = 0. \tag{5.14}$$

Hence,

$$k_t^{(0)} + \nabla_{\mathbf{II}} \cdot \left(\frac{{k^{(0)}}^3}{3} \nabla_{\mathbf{II}} \kappa^{(0)} \right) + \left(\frac{{k^{(0)}}^3}{3} \right)_z = 0, \tag{5.15}$$

$$\Gamma_t^{(0)} = 0. \tag{5.16}$$

(5.15), is precisely the evolution equation for the tangentially-immobile model (see (4.1)).

5.2. *Numerical results*

To solve (5.1), (5.2), (5.3) and (5.4), we use the scheme described in §3. The resulting DAEs are again solved using DASPK (Li & Petzold).

Our main motivation here is to analyze the stability of the system to transverse perturbations, i.e., perturbations in the y direction. Since there is no steady state to this system to perturb around, we have to rely on our numerics to study stability. In addition, we would like to simulate some of the three dimensional structures seen in experiments near the bottom and along the sides of the film (e.g., Snow *et al.*).

For the results to follow we consider an initial shape (see figure 8)

$$k(y,z,0) = \begin{cases} 1 + \mathcal{D}z\cos(\frac{2\pi y}{L_y}), & 0 \le z \le z_1. \\ 1 + r_s - \sqrt{r_s - (z-z_1)^2}, & z_1 < z \le L_z. \end{cases} \tag{5.17}$$

where $\mathcal{D} = 0.01$, the length of the computational box in the y and z directions are given by $L_y = L_z = 37.5$, respectively and $z_1 = 36.504962$, can be thought of as the z location where the film enters the bath. The equation of the static meniscus is given by

$$r_s = \sqrt{1+s_0^2}\left(\frac{L_z - z_1}{s_0}\right), \tag{5.18}$$

where $s_0 = 10$, is the slope at the bottom of the film.

The initial concentration for Γ (figure 9) is

$$\Gamma(y,z,0) = \begin{cases} \frac{[1+\tanh(z-L_z+2.5)]}{2}\left[1 - 0.01\cos(\frac{2\pi y}{L_y})\right] & 0 \le z \le z_1 \\ 1 & z_1 < z \le L_z \end{cases} \tag{5.19}$$

The surfactant concentration is set up so that there is a strong concentration (hence, surface tension) gradient in the z direction. This concentration gradient causes the flow in the z direction, $w^{(S)}$, to reverse, i.e., move upward, seen at the bottom in figure 10. We have imposed a weak surfactant concentration gradient in the y direction with more surfactant near the dip in k and less surfactant as we go toward the sides of the film. This is consistent with an increase in surfactant concentration lowering the surface tension

in the film, hence the region where surfactant concentration is high corresponds to low surface tension. The resulting concentration gradient in the y direction drags fluid toward the sides of the film (see figure 11). This tends to reinforce the existence of thick regions of the film as we shall see later on. This choice of this initial surfactant concentration can be physically realized by considering rapid withdrawl of films from the bath. We have also computed solutions for linear initial surfactant profiles corresponding to a more gradual withdrawl of films; the long time behavior of the film profiles is not strongly affected by the choice of the initial concentration.

We have used a 200×80 grid as our finite difference mesh, i.e., 200 points in the z direction and 80 in the y direction. All computations as before have been done in parallel on a SGI Origin 2000 workstation with 4 300-MHz IP27 processors. These results are computed only on coarse meshes owing to the finite difference approximations becoming unstable for fine meshes; work is currently being done to implement differencing formulas that are stable for reasonably fine meshes.

There are are a number of parameters that appear in our model; the idea is to find a parameter range that best depicts any instability mechanism or any of the experimentally observed structures. We will concentrate on a parameter regime which we believe explains the hydrodynamic instability mechanism reported previously by many authors (Baets & Stein; Hudales and Stein; Stein; Joye, Hirasaki & Miller). For the simulations depicted in this section the choice of the parameters are

$$\mathcal{S} = 10^2, \quad \bar{\mathcal{S}} = 10, \quad \mathcal{M} = 50 \quad \text{and} \quad Pe = 10^4. \tag{5.20}$$

The choice of the above parameters has been influenced by an instability criterion derived by Joye *et al.* This will be discussed in some detail in §6.

Figures 12, 13, 14 and 15 show k, Γ, $w^{(S)}$ and $v^{(S)}$, respectively, at time $t \approx 50$. We observe the first signs of the occurrence of an instability. The thickness variation in

the y direction is more prominent than before. This is caused by the Marangoni effect (surface tension gradients) in the y direction as seen from the plot for Γ (see figure 13). This instability can be explained via figure 16. Point B represents the thinner middle region of the film where Γ is high, hence the surface tension in that region is low. Point A represents the thicker region near the sides of the film where Γ is low, hence the surface tension in that region is high. These surface tension gradients cause the surface fluid to flow from thin to thick parts of the film near the top (see figure 14). At the bottom, there is a flow from the thicker to the thinner parts of the film because the surface concentration gradients are reversed there. In the middle of the film with respect to y, the surfactant concentration gradients continue to drag fluid up the surface of the film. This sets up a pair of vortices which develops behind the wave and propagates up the film. Surface tension gradients competing with gravity are the mechanisms that drives this instability. A similar Marangoni-driven instability mechanism has been observed and simulated by Joye *et al.* A more detailed discussion of their observations and some comparison with our work will be made in §6. Figure 13 for the surfactant concentration, Γ, clearly depicts the scenario explained above. The recirculation cell forming in figures 14 and 15 for the surface velocity components, is now much stronger than before. Flow is downward along the sides which implies that gravity is dominant over the Marangoni effect (gravity is dominant in the thicker parts), while flow is upward in the middle (Marangoni effect is dominant).

Figures 17, 18, 19 and 20 show k, Γ, $w^{(S)}$ and $v^{(S)}$, respectively, at time $t \approx 64$. From the free surface shape profile (figure 17), we observe that the thinner parts are now larger in the middle region of the film and the thicker parts are now more localized toward the edges of the film. This is again driven by surface tension gradients which are now more pronounced due to a larger variation in Γ across the film (see figure 18). The

recirculation cell seen in figures 19 and 20 for the surface velocity components is more prominent than before. The upward flow in the middle is now much stronger and the flow is still downward along the sides; the trends described for the previous plots have continued.

Figures 21, 22, 23 and 24 show k, Γ, $w^{(S)}$ and $v^{(S)}$, respectively, at a still later time, $t \approx 100$. The thicker film regions are now very localized at the edges of the film. The middle region is now more or less uniformly thin; from the concentration profile (figure 22) we observe that the surface tension gradients are confined to the edges of the film and is almost negligible for most part of the middle region of the film, which explains the localization near the edges (see figure 21). The surface velocity profiles (figures 23 and 24) basically depict the same scenario seen at earlier times.

Thus, from the above numerical results we have seen an instability driven primarily by surface tension gradients which cooperates with with the underlying gravity-driven bulk flow. This sort of behavior qualitatively matches some special structures observed in experiments by Snow *et al.*, but more work is needed to quantify this behavior and compare with their experiments. For example, a single vortex that fills the wire frame has been observed for one experiment; we should be able to recover this with appropriate initial conditions and parameter values. We believe that a more refined parameter search and computations with different initial conditions has to be conducted to get a closer match to experimental observations. Also, our numerics should be carried out on a more refined mesh to facilitate better comparison with experiments. This is beyond the results in this paper because of the limitations of both our computing power and the model formulation. This will form part of our work in the immediate future.

6. Comparison with Joye, Hirasaki & Miller

In a series of papers, Joye *et al.*, studied the drainage in horizontal, circular films. They have looked at both axisymmetric and symmetric drainage between the thick dimple region in the middle of the film and the thinner barrier ring Plateau border region near its edge. Some of the salient features of their experimental observations and numerical experiments follows.

They found that symmetric drainage was associated with rigid films (large surface viscosity) and asymmetric drainage with mobile films (low surface viscosity). They also found that asymmetric drainage in circular films was much more rapid than when it is axisymmetric. They proposed that this asymmetric drainage seen in circular films, marginal regeneration in vertical, rectangular films observed by Mysels *et al.* and Hudales & Stein were attributed to a hydrodynamic instability explained by Stein.

They developed a stability criterion for the onset of asymmetric drainage from a linear stability analysis. Their linear stability analysis shows that the instability is a hydrodynamic instability produced by a surface tension-driven flow. This is opposed by surface viscosity, surface diffusivity and system dimensions (wavelength of transverse perturbations, length of computational box, etc.) which stabilize perturbations having short wavelengths. They have also performed a numerical simulation of this instability, which apparently confirms the conditions for applicability of their simplified linear stability analysis, recirculation cells that have been observed experimentally and the rapid increase in drainage rate when the instability occurs.

Our problem differs from theirs in the sense that we are studying vertical drainage in mobile films wherein gravity plays a very important role. Gravity and the Marangoni effect are the main competing factors here which generate the localized thicker and thinner regions that are very similar to the periodic convection patterns seen in vertical

soap films (Mysels *et al.*). The surface tension driven instability that we numerically simulated is very similar to that observed and analyzed by Joye *et al.* These effects that we observe are primarily caused by the redistribution of surfactant due to surface and underlying bulk flows so we agree with Joye *et al.*

One of their main assumptions in performing a linear stability analysis, and then verifying it with numerical simulations, is the existence of a steady base state and that the instability develops rapidly compared to changes in film shape caused by continuous drainage. This assumption is reasonable for the horizontal ring apparatus for at least some aqueous films. We do not assume any steady state or any other restriction for the onset of instability and we impose the transverse perturbations to see whether any instability develops or not. In this sense our problem is more complete, and this is particularly needed early in the evolution when the drainage is rapid. Some difficulty arises because the drainage for mobile films is so rapid that any transverse perturbation may get washed out very quickly. However, the similarity of the results presented here with their results highlights the success of their assumptions in many instances.

Joye *et al.*'s stability criterion did give us a rough parameter range to investigate for which an instability could arise; this is precisely what motivated us to investigate the parameters used in the simulations described in the previous section. If we identify gravity as the pressure gradient and using their assumption for $\partial\Gamma/\partial x$ (very small compared to the uniform concentration of surfactant present in the absence of flow), then their stability criterion is

$$\left(\frac{2\pi}{\lambda}\right)^6\left(\frac{\mathcal{D}_s\mu^{\mathbf{s}}\bar{\sigma}_m}{\rho^2g^2}+\frac{\bar{\sigma}_m d\mu^{\mathbf{s}}\bar{\Gamma}_m(\frac{\partial\bar{\sigma}}{\partial\bar{\Gamma}})}{3\mu\rho^2g^2}\right)+\left(\frac{2\pi}{\lambda}\right)^8\left(\frac{\mathcal{D}_s\mu^{\mathbf{s}}(\kappa^{\mathbf{s}}+\mu^{\mathbf{s}})d\bar{\sigma}_m}{3\mu\rho^2g^2}\right)$$

$$\begin{cases} > 1, & \text{stable}, \\ = 1, & \text{marginal}, \\ < 1, & \text{unstable}, \end{cases} \tag{6.1}$$

in terms of our parameters. The nondimensional form of the above equation is

$$\frac{K^6 \bar{\mathcal{S}}}{\delta^{12} Pe} \left(1 + \frac{1}{3} \mathcal{M} Pe + \frac{1}{3} \frac{K^2 \mathcal{S}}{\delta^4} \right) \begin{cases} > 1, & \text{stable}, \\ = 1, & \text{marginal}, \\ < 1, & \text{unstable}, \end{cases} \tag{6.2}$$

where $K = 2\pi d/\lambda$. For the results of figures 8– 24 we find that (6.1) is less than one. One of our goals in the near future is to investigate their conditions more fully and compare parameter regimes where instability occurs.

7. Conclusions

We have formulated a 2+1 dimensional model to the study the role of finite surface viscosity, the Marangoni effect and insoluble surfactant in understanding the draining of a vertically-aligned thin liquid free film. We have used lubrication theory to derive a system of four nonlinear coupled PDEs describing the evolution of the free surface, the surface velocities and the surfactant concentration. These equations have been derived at leading order.

In order to get a simple understanding of this model both in terms of the physics and in the numerical implementation, we first studied the tangentially-immobile model. We used second order accurate finite difference schemes for the spatial discretization and solved the resulting differential-algebraic equations using DASPK. Our numerical results confirmed the fact that the surface viscosities have a stabilizing influence on transverse perturbations due to their energy dissipating effect.

Next, we studied the more complex mobile film model. The problem was again spatially

discretized by second order accurate finite difference formulas and solved using DASPK. Numerical experiments were performed on this model to understand the response of the system to perturbations across the film and to recover any experimentally observed structures. We did a limited parameter search to find a set of parameters which qualitatively depicts some of the instabilities seen in experiments.

We found an instability, very similar to that reported by Joye *et al.* who studied drainage in horizontal circular films. From our simulations we observed localized thicker and thinner regions in the film which look similar to the periodic convection patterns known as marginal regeneration seen in vertical soap films (Mysels *et al.*). We concluded that these were caused by a competition between gravity and the Marangoni effect; the underlying mechanism being the redistribution of surfactant due to the surface velocities and the underlying bulk flow. This surface tension driven instability has been reported previously by many authors. Although we were successful in simulating this instability, we are far from recovering some of the experimental structures seen in experiment, in particular, the localized structures seen at the bottom of the film. We believe that a more refined parameter search and the use of more realistic surface properties (Naire, Braun & Snow 2001) will get us closer to experiment. Also, we have not been successful in running our numerics on very fine meshes due to a breakdown of the numerics at very late times. This could be due to the boundary conditions at the bottom of the film; more investigation is needed to determine whether this is the case. This again will be part of our immediate future research; this will enable us to better quantify the comparison between our numerical computations and experiment.

Acknowledgments

RJB gratefully acknowledges support from the NSF via DMS-9620392, DMS-9722854 and DMS-9631287; RJB and SN gratefully acknowledge partial support from Dow Corning. The authors thank A. Hirsa, J. Lopez, U.C. Pernisz and B. Nugent for many useful and stimulating discussions.

REFERENCES

Baets, P. J. M. & Stein, H. N. 1994 Surface Rheology of Surfactant Solutions Close to Equilbrium. *J. Colloid Interface Sci.* **162**, 402–411.

Boussinesq, M. J. 1913 Sur l'existance d'une viscosite' superficielle, dans la mince couche de transistion separant un liquide d'une autre fluide contigu. *Ann. Chim. Phys.* **29**, 349–357.

Braun, R. J., Snow, S. A. & Pernisz, U. C. 1999 Gravitational Drainage of a Tangentially-Immobile Thick Film. *J. Colloid Interface Sci.* **219**, 225–240.

Brennan, K. E., Campbell, S. L. & Petzold, L. E. 1996 *Numerical Solution of Initial-Value Problems in Differential-Algebraic Systems.* Philadelphia:SIAM.

Edwards, D. A., Brenner, H. & Wasan, D. T. 1991 *Interfacial Transport Processes and Rheology.* Boston: Butterworth-Heinemann.

Edwards, D. A. & Oron, A. 1995 Instability of a non-wetting film with interfacial viscous stress. *J. Fluid Mech.* **298**, 287–309.

Hudales, J. B. M. & Stein, H. N. 1989 Profile of the Plateau Border in a Vertical Free Liquid Film. *J. Colloid Interface Sci.* **137**, 512–526.

Hudales, J. B. M. & Stein, H. N. 1990 Marginal Regeneration of a Mobile Vertical Free Liquid Film. *J. Colloid Interface Sci.* **138**, 354–364.

Ida, M. P. & Miksis, M. J. 1998*a* The Dynamics of thin films I: General theory. *SIAM J. Appl. Math.* **58** (2), 456–473.

Ida, M. P. & Miksis, M. J. 1998*b* The Dynamics of thin films II: Applications. *SIAM J. Appl. Math.* **58** (2), 474–500.

Joye, J. L., Hirasaki, G. J. & Miller, C. A. 1992 Dimple Formation and Behavior During Axisymmetrical Foam Film Drainage. *Langmuir* **8**, 3083–3092.

Joye, J. L., Hirasaki, G. J. & Miller, C. A. 1994 Asymmetric Drainage in Foam Films. *Langmuir* **10** (9), 3174–3179.

Joye, J. L., Hirasaki, G. J. & Miller, C. A. 1996 Numerical Simulation of Instability Causing Asymmetric Drainage in Foam Films. *J. Colloid Interface Sci.* **177**, 542–552.

Kelly, C. T. 1995 *Iterative Methods for Linear and Nonlinear Equations*. Philadelphia:SIAM.

Kheshgi, H. S., Kistler, H. S. & Scriven, S. F. 1992 Rising and falling film flows: Viewed from a first order approximation. *Chem. Engrg. Science* **47**, 683–694.

Li, S. & Petzold, L. E. 1999 Design of New DASPK for Sensitivity Analysis. *Tech. Rep.*. University of California, Santa Babara.

Mysels, K. J., Shinoda, K. & Frankel, S. 1959 *Soap Films: A Study of their Thinning and a Bibliography*. Pergamon Press, Elmsford, New York.

Naire, S., Braun, R. J. & Snow, S. A. 2000*a* An Insoluble Surfactant Model for a Vertical Draining Free Film. *J. Colloid Interface Sci.* **230**, 91–106.

Naire, S., Braun, R. J. & Snow, S. A. 2000*b* Limiting Cases of Gravitational Drainage of a Vertical Free Film for Evaluating Surfactants. *SIAM J. Appl. Math.* **61** (3), 889–913.

Naire, S., Braun, R. J. & Snow, S. A. 2001 An Insoluble Surfactant Model for a Vertical Draining Free Film with Variable Surface Viscosity. Phys. Fluids, to appear.

Nierstrasz, V. A. & Frens, G. 1998 Marginal Regeneration in Thin Vertical Liquid Films. *J. Colloid Interface Sci.* **207**, 209–217.

Nierstrasz, V. A. & Frens, G. 1999 Marginal Regeneration and the Marangoni Effect. *J. Colloid Interface Sci.* **215**, 28–35.

Ruschak, K. J. 1978 Flow of a falling film into a pool. *AIChE Journal* **24**, 705–708.

Saad, Y. 1996 *Iterative Methods for Sparse Linear Systems*. New York:PWS.

Scriven, L. E. 1960 Dynamics of a fluid interface: Equation of motion for Newtonian surface fluids. *Chem. Engrg. Science* **12**, 98–108.

Slattery, J. C. 1990 *Interfacial Transport Phenomena*. New York: Springer-Verlag.

Snow, S. A., Nugent, B. M. & Pernisz, U. C. 1996*a* Cell Opening in Polyurethane

Foams Part IV: The Effect of Surfactant Concentration and Structure on Thin Liquid Polyurethane Films. *Tech. Rep.* 1996-I0000-42521. Dow Corning Corporation, manuscript for external publication in preparation.

Snow, S. A., Nugent, B. M. & Pernisz, U. C. 1996*b* Cell Opening in Polyurethane Foams Part V: Model Polyurethane Films Stabilized by DC 407 Resin. *Tech. Rep.* 1996-I0000-42699. Dow Corning Corporation, manuscript for external publication in preparation.

Snow, S. A., Nugent, B. M., Pernisz, U. C., Naire, S. & Braun, R. J. 1996*c* Cell Opening in Polyurethane Films Part III: The Drainage of Thin Liquid Model Polyurethane Films. *Tech. Rep.* 1996-I0000-41395. Dow Corning Corporation, manuscript for external publication in preparation.

Snow, S. A., Pernisz, U. C. & Stevens, R. E. 1998 Thin Liquid Model Polyurethane Films. In *Polyurethane World Congress, Paper C4*, pp. 1–10.

Snow, S. A. & Stevens, R. E. 1999 *The Science of Silicone Surfactant Application in the Formation of Polyurethane Foam*, *Surfactant Science Series*, vol. 86, chap. 5 in *Silicone Surfactants*, pp. 137–158. New York: Marcel Dekker.

Stein, H. N. 1991 On Marginal Regeneration. *Advances in Colloid and Interface Sci.* **34**, 175–190.

Stone, H. A. 1990 A simple derivation of the time-dependent convective-diffusion equation for surfactant transport along a deforming interface. *Phys. Fluids A* **2**, 111–112.

Wilson, S. D. R. 1982 The Drag-out Problem in Film Coating Theory. *J. Engrg. Math.* **16**, 209–221.

Wong, H., Rumschitzki, D. & Maldarelli, C. 1996 On the surfactant mass balance at a deforming fluid interface. *Phys. Fluids* **8**, 3203–3204.

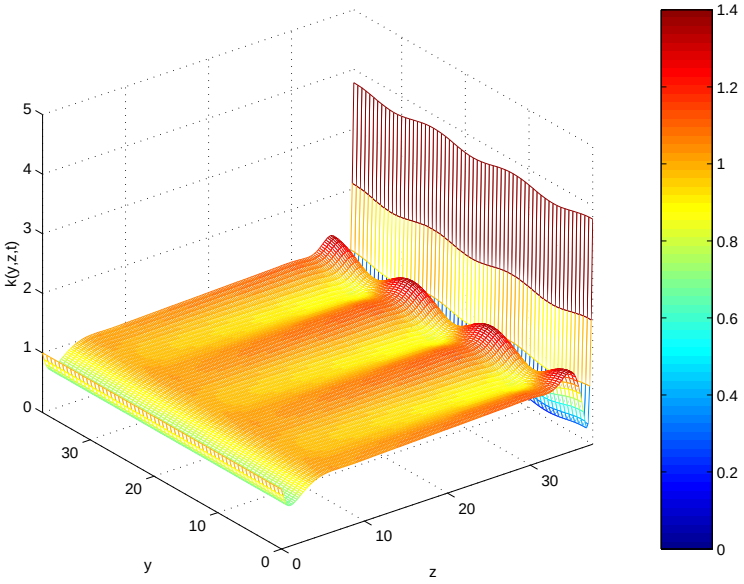

FIGURE 4. Free surface shape k at $t = 2$. Perturbations are still almost the same magnitude as initial shape. The static meniscus approximation becomes more one dimensional as the calculation progresses.

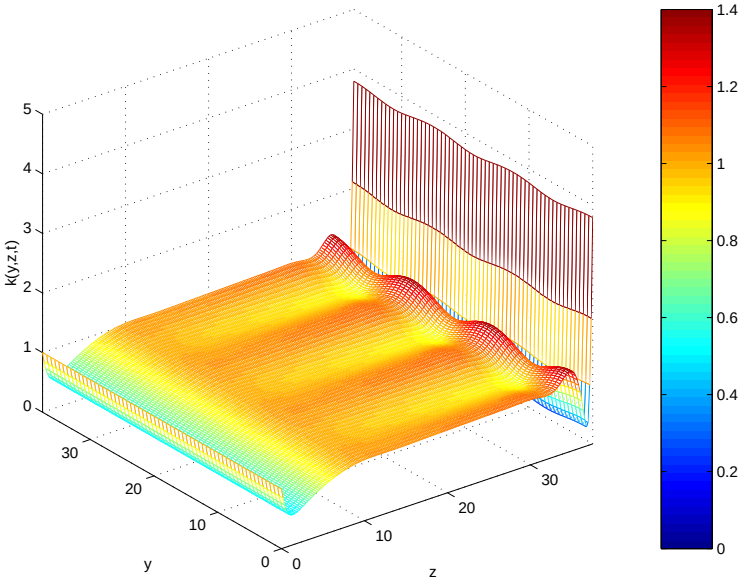

FIGURE 5. Free surface shape k at $t = 6$. The bumps near the bottom are slowly decaying and we see the meniscus is rapidly forming at the top. The concave-in profile in the middle region is again consistent with 1+1 dimensional results.

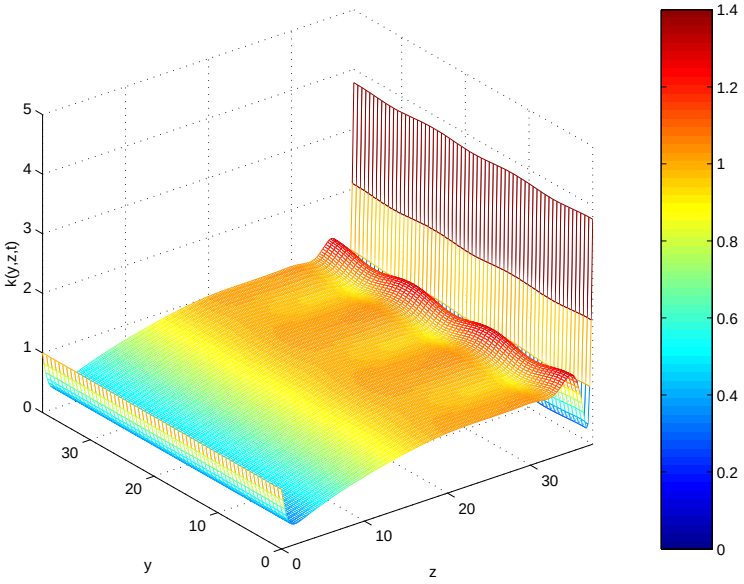

FIGURE 6. Free surface shape k at $t = 16$. The bumps near the bottom are getting much smaller than before.

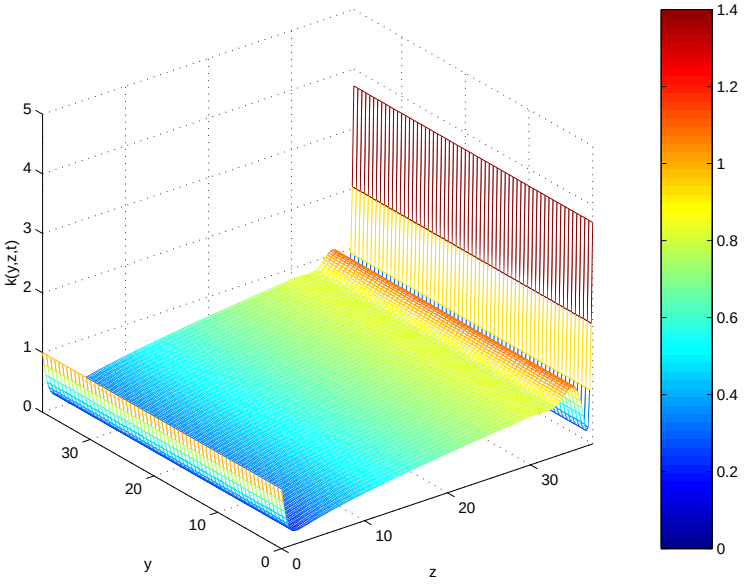

FIGURE 7. Free surface shape k at $t = 45$. The bumps have all decayed and the one dimensional meniscus approximation is excellent. We expected the perturbations to decay since this is the limiting case when $\bar{\mathcal{S}} \to \infty$ (see §5.1).

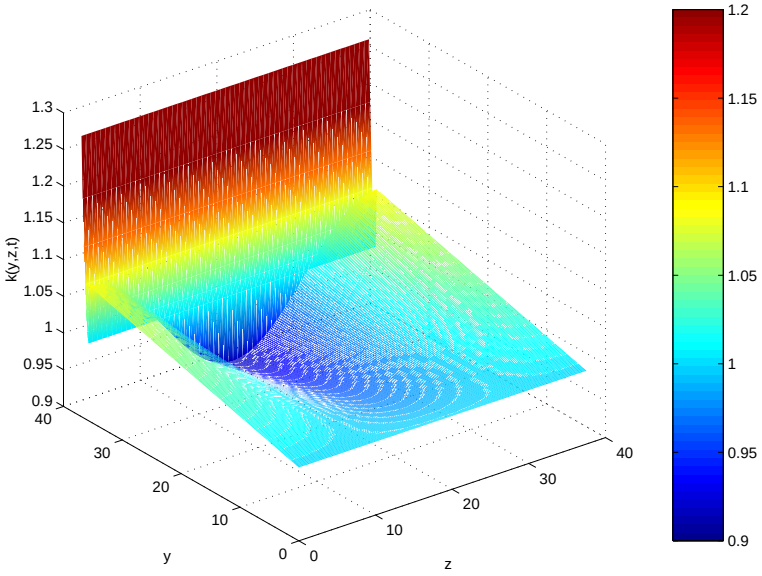

FIGURE 8. Initial free surface shape $k(y, z, 0)$. Perturbations in the y direction have been imposed on the initial shape according to Equation (5.17).

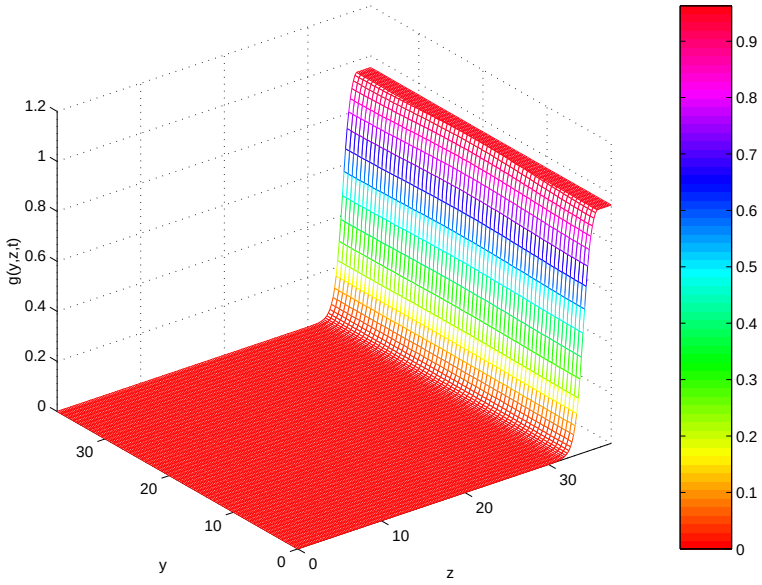

FIGURE 9. Initial surfactant concentration $\Gamma(y, z, 0)$. There is a strong concentration gradient in the z direction close to the bottom of the film; a weak concentration perturbation in the y direction has also been imposed in this region; it is given by Equation (5.19).

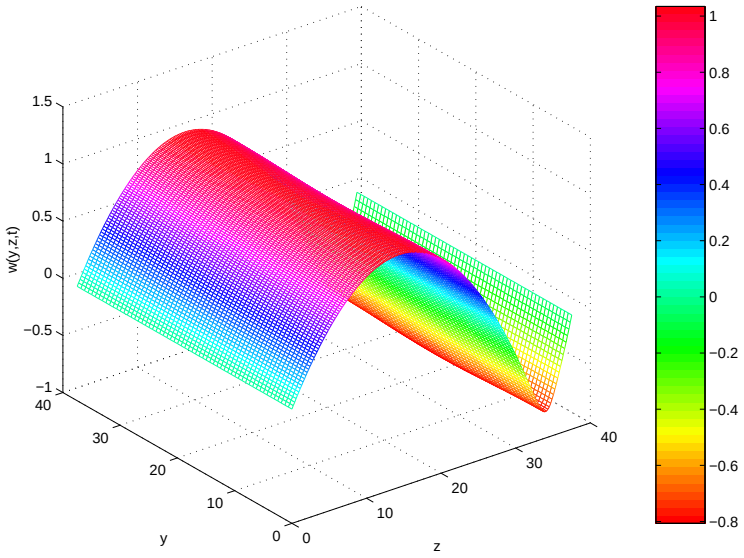

FIGURE 10. Initial surface velocity in the z direction, $w^{(S)}(y, z, 0)$. There is a reversal of flow close to the bottom of the film, this is due to strong concentration gradients in z near that region (see figure 9).

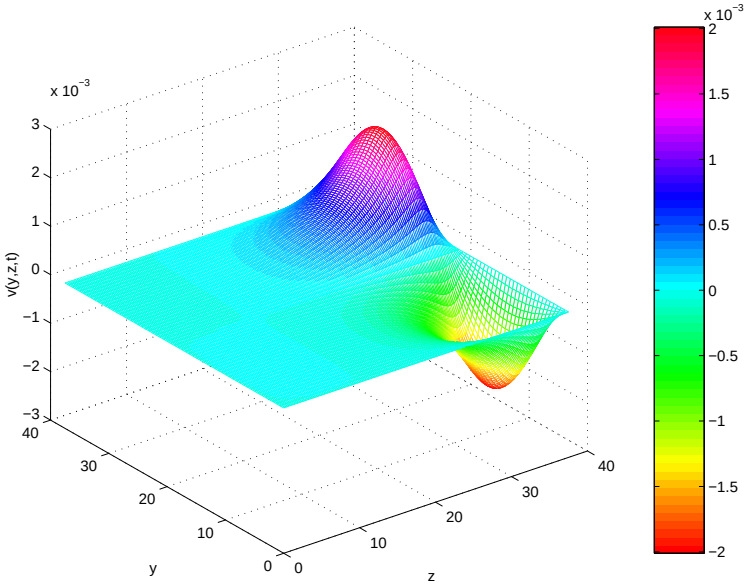

FIGURE 11. Initial surface velocity in the y direction, $v^{(S)}(y, z, 0)$. The flow in this region is moving outward to the edges of the film; this is due to surface tension gradients in the y direction near that region.

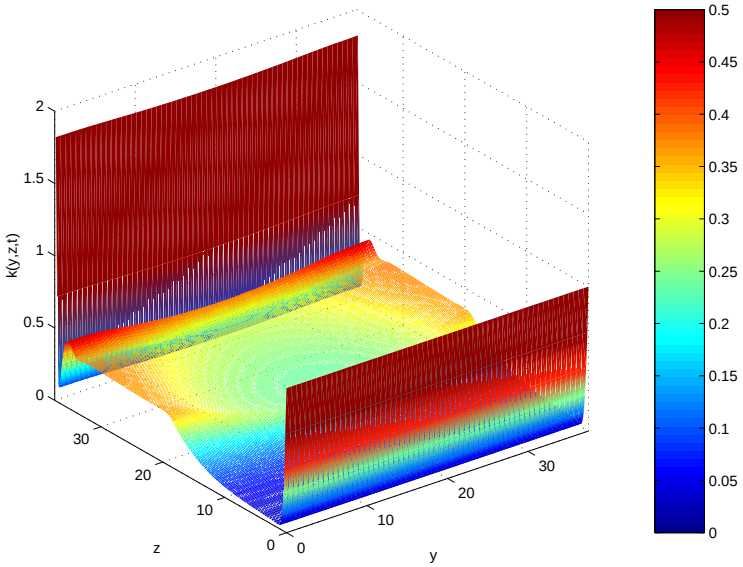

FIGURE 12. Free surface shape k at $t \approx 50$. The instability seen here is the developing of localized thick and thin regions along the y direction. This is primarily due to the interaction between the Marangoni effect (surface tension gradients) and gravity.

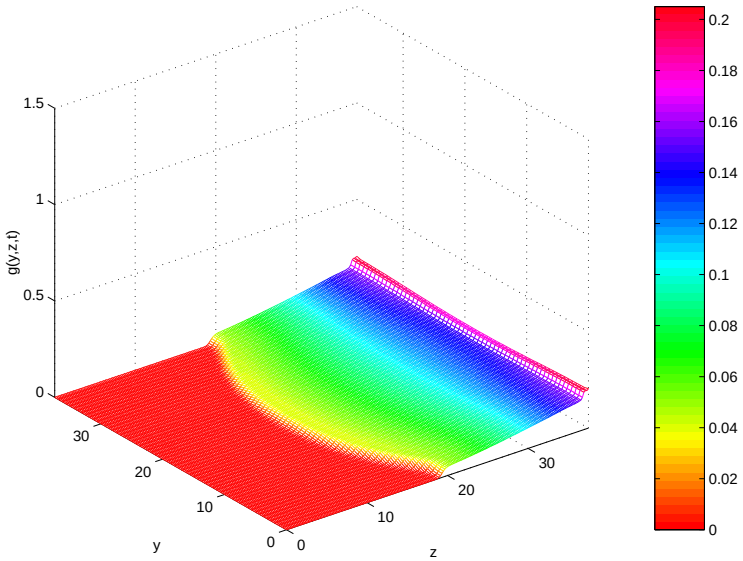

FIGURE 13. Concentration profile Γ at $t \approx 50$. Concentration gradients are still strong in the z direction and the surfactant is being dragged up the film. Concentration gradients are now much stronger in the y direction than they were initially.

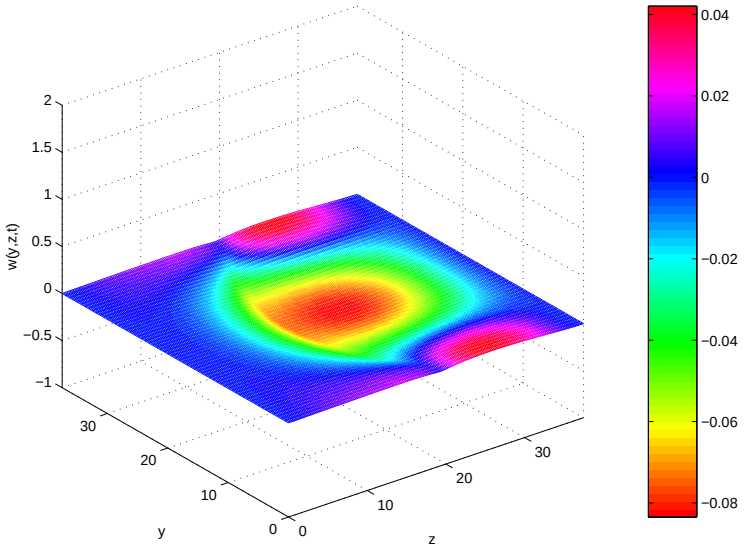

FIGURE 14. Surface velocity $w^{(S)}$ at $t \approx 50$. The recirculation region forming near the middle and bottom portions of the film is now much stronger than before. Flow is in the upward direction in the middle region (Marangoni effect dominant) and downward along the sides (gravity dominant).

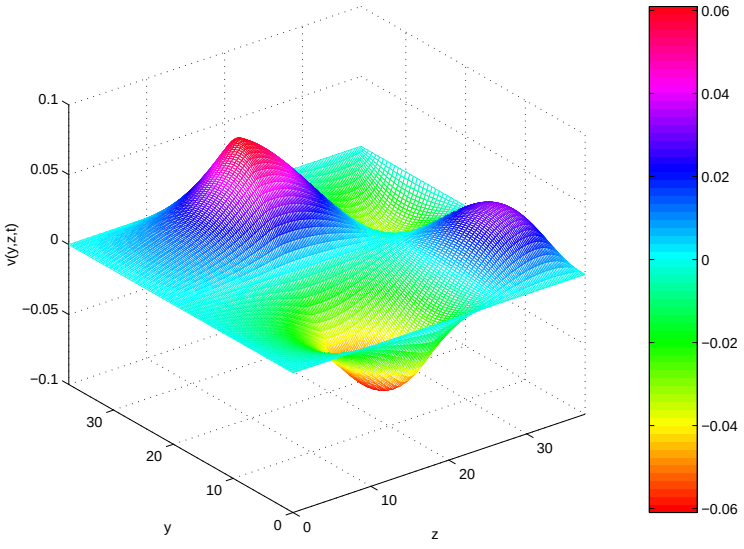

FIGURE 15. Surface velocity $v^{(S)}$ at $t \approx 50$. The outward flow is stronger due to surface tension gradients in the y direction which drags fluid to the sides of the film (see figure 13).

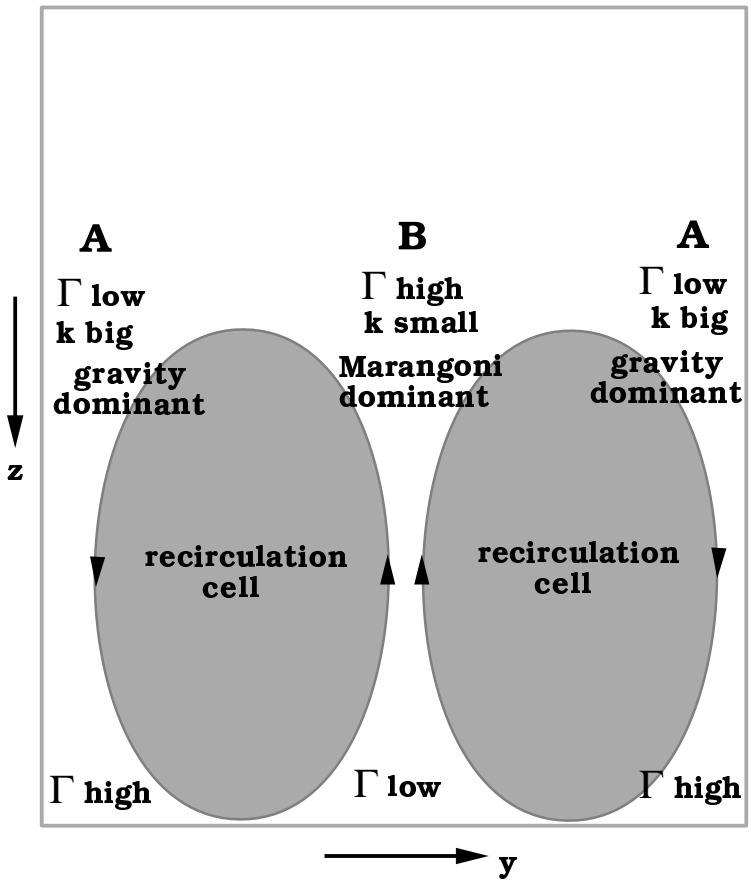

FIGURE 16. Instability mechanism. A similar mechanism was reported by Joye *et al.* (see §6).

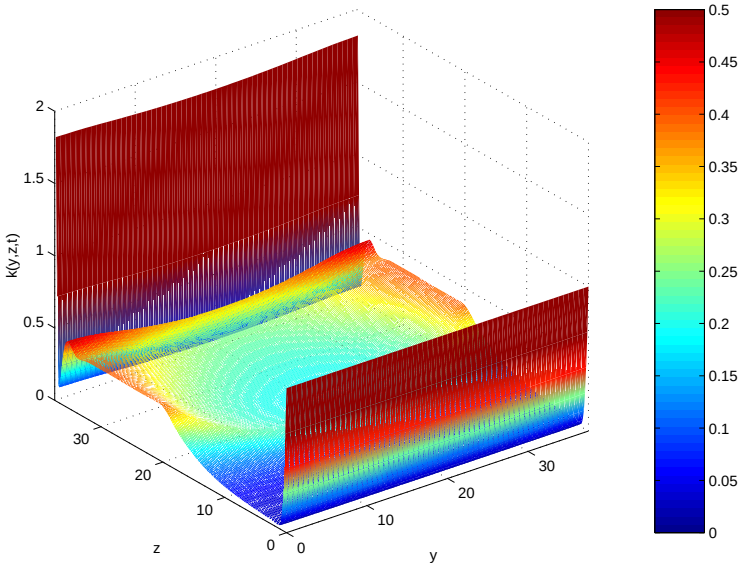

FIGURE 17. Free surface shape k at $t \approx 64$. The thick regions are now localized more along the sides of the film and the thinner parts cover most of the middle region. This is again due to the strong surface tension gradients which are now concentrated along the sides of the film (see figure 18).

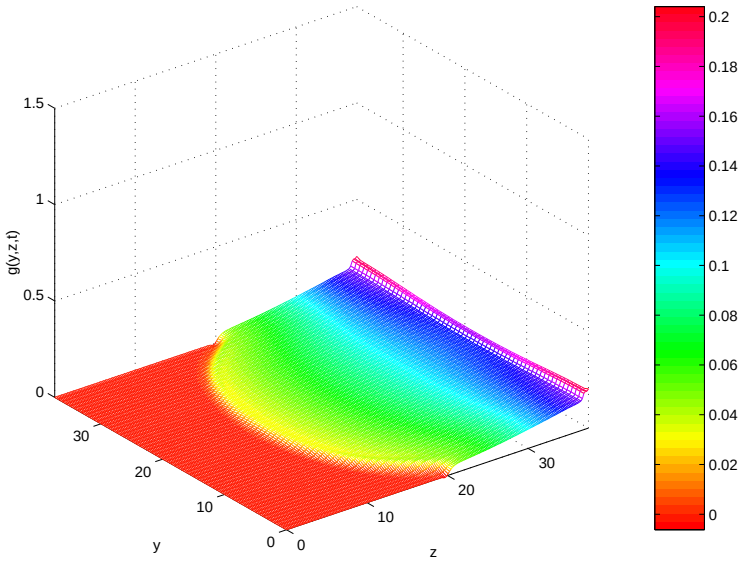

FIGURE 18. Concentration profile, Γ, at $t \approx 64$. Concentration gradients in the y direction are now much stronger along the sides of the film causing film to thin in the middle and thicken along the sides (see figure 16).

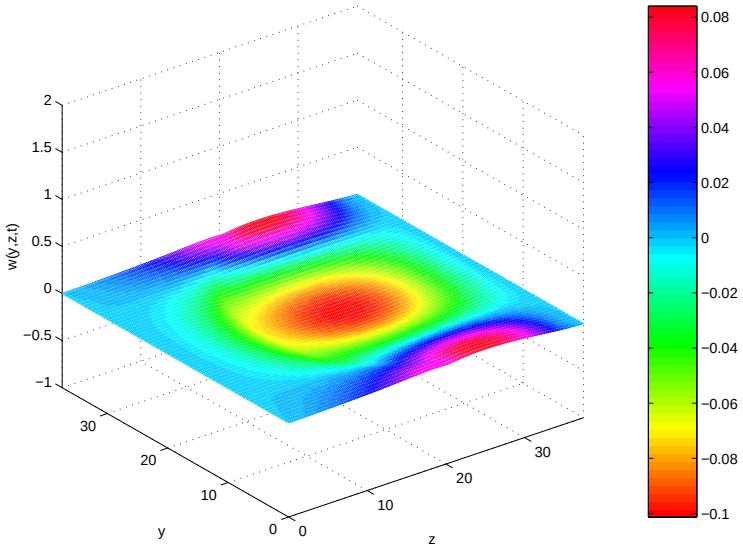

FIGURE 19. Surface velocity $w^{(S)}$ at $t \approx 64$. The recirculation region is much stronger with flow primarily in the upward direction in the middle (Marangoni effect dominant) and downward along the sides (gravity dominant).

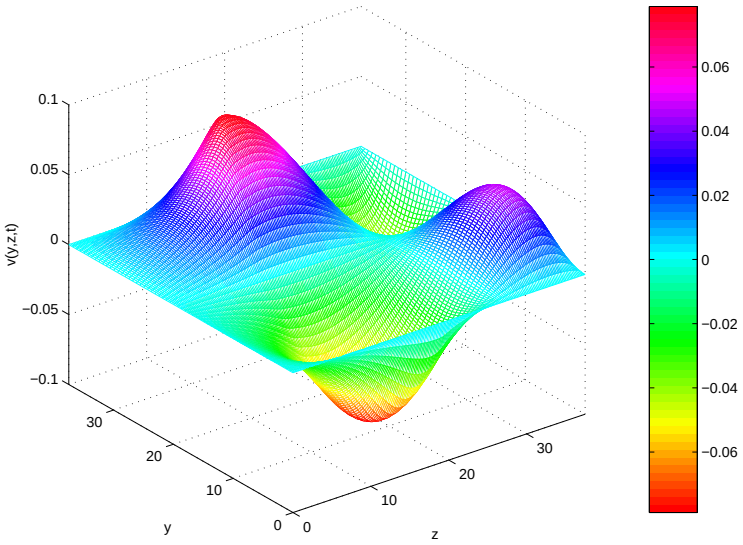

FIGURE 20. Surface velocity $v^{(S)}$ at $t \approx 64$. The outward flow is much stronger due to surface tension gradients in the y direction which drag the flow out to the sides of the film.

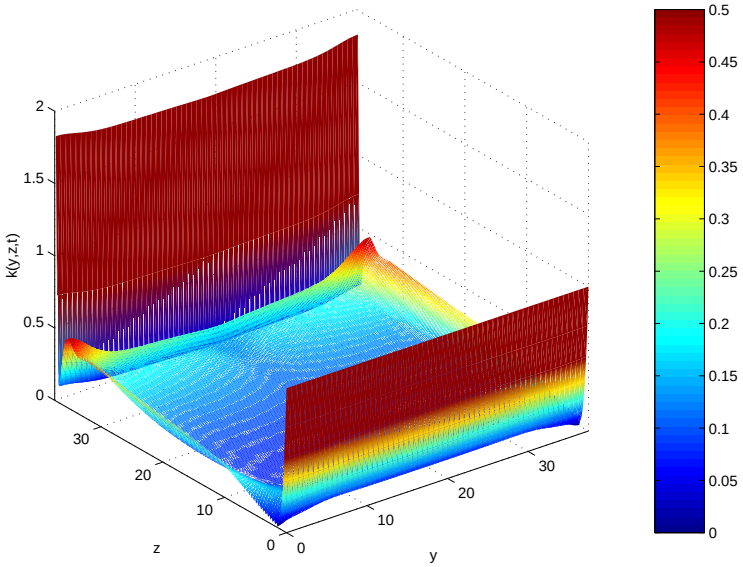

FIGURE 21. Free surface shape k at $t \approx 100$. The thicker parts of the film are now all concentrated near the edges while the middle thins in a roughly uniform way.

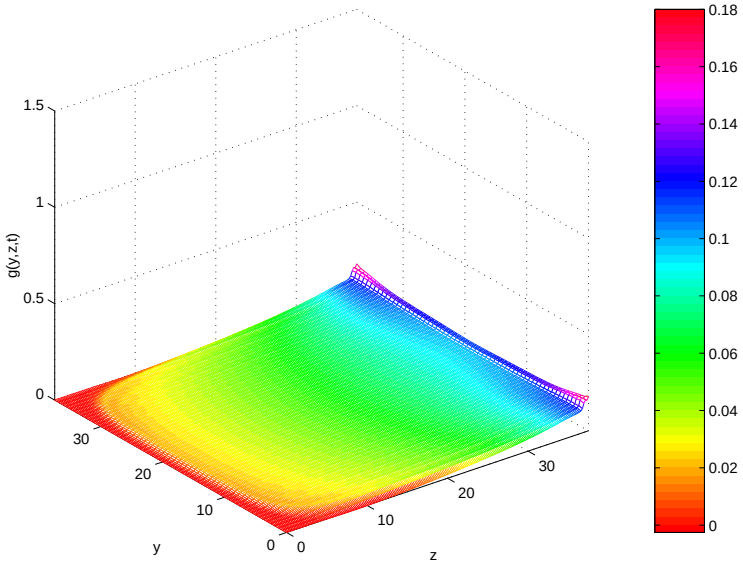

FIGURE 22. Concentration profile Γ at $t \approx 100$. Concentration gradients in the y direction are confined more to the edges of the film; towards the middle, the concentration is roughly uniform.

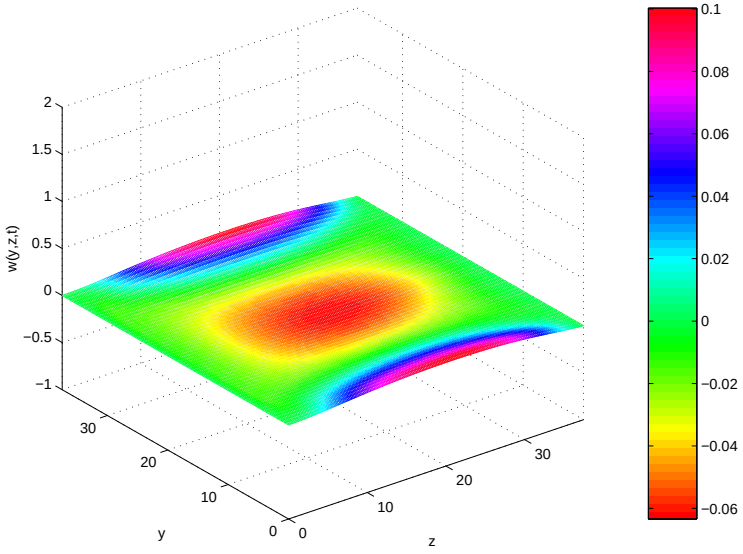

FIGURE 23. Surface velocity $w^{(S)}$ at $t \approx 100$. As before, we still see the recirculation cells; the flow is downward along the sides and upward at the middle of the film.

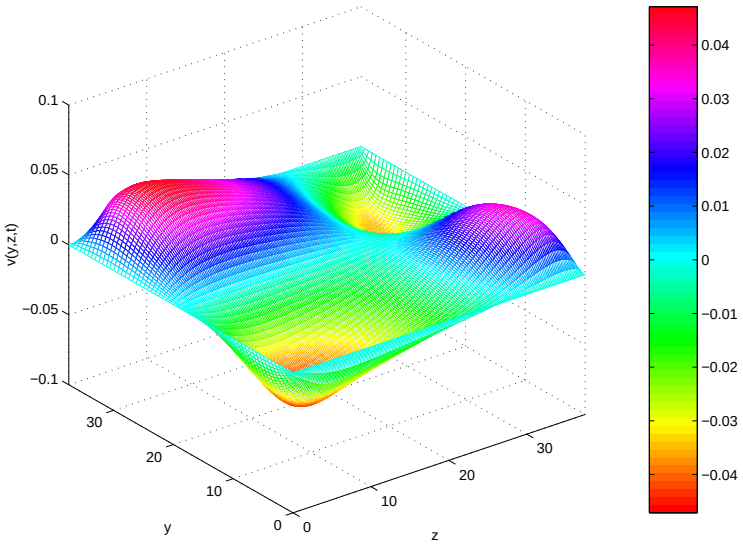

FIGURE 24. Surface velocity $v^{(S)}$ at $t \approx 100$. The outward flow has moved more towards the upper part of the film.